To bind or not to bind, that is an important question! : Development of covalent probes for adenosine receptors

Yang, X.

Chapter 2

Molecular Probes for the Human Adenosine Receptors

Xue Yang

Laura H.Heitman

Daan van der Es

Adriaan P. IJzerman

To be submitted

1. Introduction

Adenosine receptors (ARs), which are activated by their endogenous ligand adenosine, belong to the Class A family of G protein-coupled receptors (GPCRs). These receptors have been considered potential therapeutic targets in several disorders, including Parkinson's disease, schizophrenia, analgesia, ischemia and cancer [1]. To date, four subtypes of adenosine receptors have been identified, namely A_1, A_{2A}, A_{2B} and A_3. Activation of A_1 and A_3 receptors leads to inhibition of adenylate cyclase trough their interaction with a G_i protein, whereas A_{2A} and A_{2B} receptors stimulate the enzyme through a G_S-linked pathway. Until now, the 3D-structures of the A_1 and A_{2A} subtypes have been elucidated [2, 3]; studies on the A_{2B} and A_3 subtypes have yet to be successful. Although structure elucidation was relatively successful for adenosine receptors, the membrane-bound GPCRs still prove challenging due to their low expression in native tissue, and their inherent flexibility and instability once extracted from the membrane, which is often needed for further structural studies. Over the past decades a diverse array of molecular probes, bifunctional ligands that can be used to interrogate receptor structure and function, has proven invaluable in GPCR research. From a chemical perspective, a molecular probe can be defined as a small molecule that binds the receptor of interest and enables further studies by virtue of a connected tag or functional group that exhibits specific properties. These conjugated tags or functional groups include radioactive or fluorescent moieties to enable studies on ligand-receptor binding as well as the quantification and visualization of receptors. Moreover, tags containing a reactive warhead capable of irreversibly binding to the receptor have been shown to facilitate structure elucidation, and when made bifunctional, i.e. combined with a click handle, these can be used as affinity-based probes (AfBPs). It emerged as valuable tools for chemical biology or proteomics studies to gain further insight into receptor localization and target engagement [4-6]. This strategy was inspired by earlier activity-based protein profiling-click chemistry (ABPP-CC), which helped in visualizing and quantifying the activities of drug targets (mainly enzymes) in native biological systems [7, 8]. In this review, various chemical probes for human adenosine receptors will be summarized. where we will limit this review to molecular probes compromising radioligands, fluorescent ligands and covalent ligands.

2. Radioligands for *in vitro* characterization

Some adenosine receptor agonists and antagonists have been developed in a radiolabeled ('hot') form, so-called radioligands. Often, these are high affinity molecules containing radioactive isotopes such as [^{3}H]-, [^{125}I]-, and [^{35}S]-, which emit radiation that can be detected

and quantified. The majority of radioligands used for *in vitro* assays are labeled with either [^{125}I]- or [^{3}H-. [^{125}I]-labeled ligands show a higher specific activity (~2,000 Ci/mmol) and shorter half-life ($t_{1/2}$ = 60 days) compared to tritium-labeled ligands (specific activity ~ 25-120 Ci/mmol and $t_{1/2}$ = 12.5 years), where the latter are more biologically indistinguishable from the unlabeled parent ligand. These radiolabeled ligands are predominantly used in saturation experiments to measure the radioligand's equilibrium dissociation constant, K_D, and receptor expression/density (B_{max}), in competition displacement experiments to determine the affinity (equilibrium inhibitory constant K_i) of non-labelled ('cold') compounds, and in binding kinetics assays to determine a ligand's association (k_{on}) and dissociation (k_{off}) rate constants [9, 10]. Conventional radioligand binding assays require a filtration step to separate bound from unbound radiolabeled ligands and capture the radioligand-receptor complex. A more recently developed bead-based assay, the scintillation proximity assay (SPA), has emerged as a rapid and sensitive assay to perform high throughput screens in a homogeneous system. Due to the diverse applicability of these techniques in receptor research, a diverse set of radioligands for the different AR subtypes has been developed. All radioligands that are currently commonly used are summarized in Table 1.

2.1. Radioligands for the adenosine A_1 receptor

The initial agonist radioligands for A_1R were all tritiated adenosine-based derivatives. Among them [^{3}H]CCPA (Fig. 1; Table 1) showed highest affinity with a K_D value of 0.61 nM for human A_1R (hA_1R) [11]. [^{3}H]LUF5834 is a non-nucleoside partial agonist radioligand (Fig. 1; Table 1) with nanomolar affinity (K_D = 2.03 ± 0.52 nM) for the hA_1R [12]. Its partial agonistic nature allows this radioligand to bind to both G protein-coupled and -uncoupled receptors. This radioligand proved a versatile tool to estimate the efficacy and the mechanism of action of both agonists and inverse agonists at the hA_1R.

The reference antagonist radioligand for A_1R is the xanthine-derived antagonists/inverse agonist [^{3}H]DPCPX (Fig. 1; Table 1) [13]. Although this xanthine derivative displays lower affinity at the human (K_D = 3.86 nM) [13] than the rat receptor (K_D = 0.18 nM) [14], it is still a very useful tool for the characterization of A_1R and consequently discriminate from other subtypes. It has been applied to SPA technology, constituting an alternative platform for real-time measurements of receptor-ligand interactions on hA_1R [15]. Antagonist radioligands instead of agonists tend to label all receptors present in a cell membrane preparation independent of their coupling to a G protein and are therefore used more frequently in AR research, and GPCR research in general.

2.2. Radioligands for the adenosine A_{2A} receptor

The reference radioligands for binding assays at $A_{2A}R$ include the adenosine-based agonists [^{3}H]NECA (Fig.1 ; Table 1) [13] or [^{3}H]CGS21680 (Fig. 1; Table 1) [16]. [^{3}H]NECA bound to $hA_{2A}R$ with a K_D-value of 20.1 nM. However, this non-selective radioligand also exhibited remarkably high affinity for hA_3R with a K_D-value of 6 nM, threefold higher than at the A_{2A} receptor [13]. Later, a more selective radioligand, [^{3}H]CGS21680 showed a moderate affinity for human $A_{2A}R$ with a K_D value of 22 ± 0.5 nM and has been used in autoradiographic studies, revealing the distribution of the $A_{2A}R$ in the basal ganglia of the human brain and an increased $hA_{2A}R$ level in the striatum of schizophrenic patients [17-19]. However, besides its agonistic binding with high and low affinity states to the receptor, application of this agonist radioligand is further limited due to complex binding characteristics related to non-A_{2A} binding sites [20] and enhanced affinity by increasing concentrations of Mg^{2+} ions [16].

To avoid the issues occurring with agonistic radioligands, two xanthine-based antagonist radioligands [^{3}H]XAC (Fig. 1;Table 1) [21] and [^{3}H]MSX-2 (Fig. 1;Table 1) [22] were developed to investigate the $A_{2A}R$. Though the unlabeled compound XAC showed poor selectivity for $hA_{2A}R$ over hA_1R (30-fold) and hA_3R (90-fold) [13], [^{3}H]XAC was used to identify the important residues involved in the $hA_{2A}R$ binding pocket with a K_D value of 9.4 ± 2.3 nM [21]. [^{3}H]MSX-2 is a styrylxanthine-based antagonist which bound selectively to $rA_{2A}R$ (K_D = 8.04 ± 2.62 nM) [22]. Furthermore, *in vitro* autoradiography using [^{3}H]MSX-2 showed the greatest binding in the striatum, which is in line with the expected density of $A_{2A}R$ in the mouse, rat and pig brain [23]. A preliminary *ex vivo* study confirmed that [^{3}H]MSX-2 penetrated the blood-brain barrier, which is promising for *in vivo* use [23]. Applications of these styrylxanthine derivatives are limited however, due to the tendency to undergo photoinduced isomerization [24]. Meanwhile, two non-xanthine antagonist radioligands were developed as well. [^{3}H]ZM241385 (Fig. 1; Table 1) showed a high affinity and low non-specific binding to $hA_{2A}R$[25, 26]. However, this radioligand also binds to $A_{2B}R$ with nanomolar affinity (K_D = 33.6 ± 2.8 nM) [27]. [^{3}H]SCH58261 (Fig. 1; Table 1) showed a better selectivity at the $hA_{2A}R$ (hA_{2B}/hA_{2A} = 8352) than [^{3}H]ZM241385 and was used in autoradiographic studies to investigate the receptor distribution in the human brain [17, 28]. Similarly, [^{3}H]SCH58261 was applied in *ex vivo* binding studies to study $A_{2A}R$ receptor occupancy of various ligands in mouse brain [29]. Additionally, this radioligand was applied to high throughput ligand screening in a SPA set-up and showed comparable sensitivity to the conventional filtration assay [30].

2.3. Radioligands for the adenosine A_{2B} receptor

So far only one selective agonist radioligand has been described for the $A_{2B}R$, which is tritium labeled BAY 60-6583 (Fig. 1; Table 1) [31]. Unfortunately, the specific binding of [^{3}H]BAY 60-6583 was too low compared to its high non-specific binding to establish a robust radioligand binding assay. Until now the non-selective agonist radioligand [^{3}H]NECA, despite its low affinity, remains the only molecular tool available to study the active $A_{2B}R$ conformation [31, 32].

The A_1R radioligand [^{3}H]DPCPX (Fig. 1; Table 1) was also reported to bind $hA_{2B}R$ (K_D = 40 nM) and has been used to determine the affinity of competing ligands [33, 34]. Another commonly used nonselective radioligand is [^{125}I]ABOPX (Fig. 1, Table 1) [35]. It bound to $A_{2B}R$ with moderate affinity (K_D = 37 nM) and showed a high specific binding to a $hA_{2B}R$ overexpressed cell line. The first $A_{2B}R$-selective antagonist radioligand is [^{3}H]MRS1754 (Fig. 1; Table 1), bound to $hA_{2B}R$ with a K_D value of 1.13 ± 0.12 nM [36]. Later, another xanthine analogue radioligand [^{3}H]MRE-2029-F20 was reported with comparable affinity and selectivity [37, 38]. Besides, the pyrrolopyrimidine-derivative, OSIP339391 (Fig. 1; Table 1), was labeled with tritium, representing a novel selective and high affinity radioligand for the $hA_{2B}R$ [39]. However, all these radioligands showed poor selectivity (less than 100-fold) toward the hA_1R. More recently, Müller *et al.* investigated the structure-activity relationships of 1-alkyl-8-(piperazine-1-sulfonyl)phenylxanthine derivatives, yielding a new and potent A_{2B}-selective antagonist, PSB-603 [40]. Tritium labeled PSB-603 (Fig. 1; Table 1) was subsequently developed and employed as the first high affinity (K_D = 0.403 nM) $A_{2B}R$-specific radioligand for receptor pharmacological studies. However, the current xanthine-based radioactive tracers are highly lipophilic compounds that exhibit unfavorable non-specific to specific binding ratios; this feature confines their application to receptor studies in isolated membranes.

2.4. Radioligands for the adenosine A_3 receptor

Initially, studies on the human A_3R (hA_3R) were performed using the non-selective agonist radioligand [^{3}H]NECA (Fig.1, Table 1) [13]. For binding studies on the rat A_3R (rA_3R), [^{125}I]I-APNEA (Fig. 1, Table 1) was the preferred radioligand [41]. Though [^{125}I]I-APNEA showed reasonable affinity for the rA_3R (K_D =15.5 ± 2.4 nM), it was shown to be even more potent for the rA_1R (K_D = 1.32 ± 0.35 nM) [41, 42]. Another agonist radioligand, [^{125}I]I-AB-MECA (Fig. 1; Table 1), showed better affinities for both rA_3R (K_D = 1.48 ± 0.33 nM) and hA_3R (K_D = 1.86 ± 0.69 nM) [42, 43], but still bound to rA_1R in nanomolar range (K_D = 3.42

± 0.43 nM) [42]. To tackle the selectivity challenge, Klotz *et al.* developed the tritiated agonist radioligand [^{3}H]HEMADO (Fig. 1, Table 1) [44], which showed high-affinity (K_D = 1.10 nM) and low non-specific binding (1-2% at K_D value) to hA_3R. Even though no binding on the rat rA_3R was observed, the enhanced selectivity versus other AR subtypes (>300 fold) made [^{3}H]HEMADO a useful tool for A_3R binding assays. Subsequent efforts in finding a selective ligand for the rA_3R resulted in [^{125}I]MRS1898 (Fig. 1; Table 1). It selectively binds to rA_3R with an improved K_D value of 0.17 ± 0.04 nM [45]. Still, there are some liabilities caused by the high non-specific binding. The truncation of the 5'-position of the ribose moiety generated the latest A_3R agonist radioligand [^{125}I]MRS5127 (Fig. 1; Table 1) with a K_D value of 5.74 ± 0.97 nM [46]. Its major advantage is the low degree of non-specific binding (27±2% at a concentration of 5 nM) and its improved selectivity versus the other AR subtypes. These benefits, together with the uniformity of its agonistic nature across species, may render [^{125}I]MRS5127 the preferred chemical tool for characterizing the A_3R in its active state over other radioligands reported previously. It is fair to say though that commercially available [^{125}I]I-AB-MECA has emerged as a reference radioligand.

Until now, only two antagonist radioligands, [^{3}H]MRE-3008-F20 (Fig. 1; Table 1) [47, 48] and [^{3}H]PSB-11 (Fig. 1; Table 1) [49], have been reported. While both derivatives selectively bind the hA_3R at (sub)nanomolar concentrations, [^{3}H]PSB-11 shows a much lower degree of non-specific binding (2.5 ± 0.1% at K_D value) than [^{3}H]MRE-3008-F20 (ca. 25% at K_D value). The shortage of these structurally diverse heterocyclic antagonists is their low affinity for the A_3R in non-human, particularly rodent tissue.

Table 1. Commonly used AR radioligands for *in vitro* studies

	Radioligands	K_D[a] (nM)	Functionality	Refs	Commercially Available
A_1					
	[^{3}H]CCPA	0.61	Agonist	[13]	Y
	[^{3}H]LUF5834	2.03	Agonist	[12, 50]	N
	[^{3}H]DPCPX	3.86	Antagonist	[13]	Y
A_{2A}					
	[^{3}H]NECA	20.1	Agonist	[13]	Y
	[^{3}H]CGS21680	22	Agonist	[19]	Y
	[^{3}H]XAC	9.4	Antagonist	[21]	N
	[^{3}H]MSX-2	8.04	Antagonist	[22]	Y
	[^{3}H]ZM241385	0.60	Antagonist	[26]	Y
	[^{3}H]SCH58261	2.3	Antagonist	[28]	Y
A_{2B}					
	[^{3}H]NECA	441	Agonist	[31]	Y
	[^{3}H]DPCPX	40	Antagonist	[33]	Y
	[^{125}I]ABOPX	37	Antagonist	[35]	N
	[^{3}H]MRS1754	1.13	Antagonist	[36]	Y
	[^{3}H]MRE-2029-F20	2.8	Antagonist	[37]	Y
	[^{3}H]OSIP339391	0.17	Antagonist	[39]	N
	[^{3}H]PSB-603	0.403	Antagonist	[40]	N
A_3					
	[^{3}H]NECA	6.18	Agonist	[13]	Y
	[^{125}I]APNEA	15.5 (r)	Agonist	[42]	N
	[^{125}I]AB-MECA	1.86	Agonist	[43]	Y
	[^{3}H]HEMADO	1.10	Agonist	[44]	Y
	[^{125}I]MRS1898	0.17 (r)	Agonist	[45]	N
	[^{125}I]MRS5127	5.74	Partial agonist	[46]	N
	[^{3}H]MRE-3008-F20	0.80	Antagonist	[47]	N
	[^{3}H]PSB-11	4.9	Antagonist	[49]	N

[a] The data are K_D-values for radiolabeled compounds (nM) for the indicated human adenosine receptors unless a different species is indicated (r = rat). n.d. = not detectable

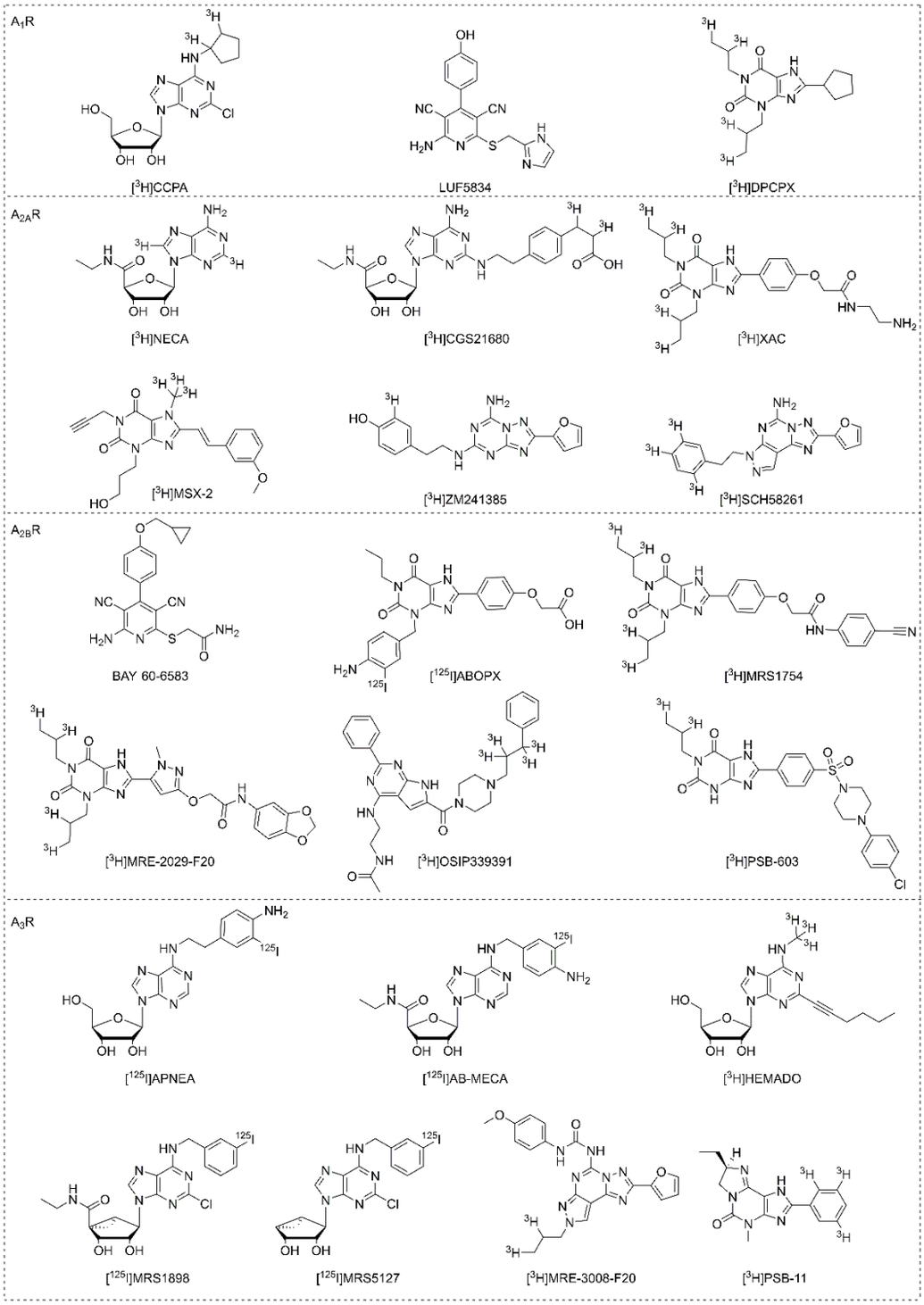

Fig. 1. Chemical structures of commonly used AR radioligands for *in vitro* studies. Note: unlabeled version was drawn for radioligands with unknown radioisotope position (i.e. [^{3}H]LUF5834 and [^{3}H]BAY 60-6583).

3. Radioligands for *in vivo* studies –PET/SPECT tracers

While β-emitting ligands serve their purpose in *in vitro* or *ex vivo* experiments, they are not suitable for *in vivo* application. To that end, positron emission tomography (PET) and single-photon emission computed tomography (SPECT) scanning have emerged and are noninvasive quantitative techniques to measure the receptor distribution and function *in vivo*. Over the years an ever-expanding library of [^{11}C]-, [^{18}F]- and [^{123}I]-labelled radiotracers has been developed that enables the determination of receptor binding potentials (BPs) in physiological and pathophysiological studies. Though the decay of these isotopes is much faster than is the case for [^{3}H]- or [^{125}I]-labeled ligands, the relatively safe γ- and photon-emissions make these tracers suitable for physiological applications. SPECT radioisotopes, such as γ-emitting [^{123}I] ($t_{1/2}$ = 13.2 hours), typically have a much longer half-life than PET tracers labeled with [^{11}C] ($t_{1/2}$ = 20.3 minutes) or [^{18}F] ($t_{1/2}$ = 110 minutes), which allow for longer radiosynthetic protocols and enables SPECT imaging to be conducted for longer time periods. Nonetheless, PET studies of adenosine receptors have been more widely performed due to the higher resolution and sensitivity that can generally be achieved compared to SPECT. In the development of radiotracers for ARs, particularly in the brain and central nervous system, it is desirable to not only optimize for affinity and low non-specific binding capacity, but also for blood−brain barrier permeability. A major challenge is that the short radioligand half-life requires on-site synthesis and rapid purification and validation of the probes. PET and SPECT imaging times, which are also related to radioligand $t_{1/2}$, are usually insufficient to allow radioligand–receptor binding to reach an equilibrium; therefore, appropriate kinetic models should be used to correct for this shortcoming. PET imaging of ARs *in vivo*, and the applications thereof in drug discovery have been comprehensively reviewed [51-53]. Here we will focus on the recent applications of clinical PET imaging studies on ARs.

3.1. PET tracers for the adenosine A_1 receptor

Two xanthine derivatives, [^{18}F]CPFPX (Fig. 2, Table 2) and [^{11}C]MPDX (Fig. 2, Table 2), have been extensively employed for the characterization of A_1R in human brain and their results summarized in several reviews [51, 54]. While [^{18}F]CPFPX has a higher affinity for A_1R than [^{11}C]MPDX, the latter has been shown to be much more stable againstperipheral metabolism. Using these PET tracers, the cerebral distribution of the A_1R has been successfully visualized and quantified in human brain [55, 56]. From these studies a correlation between A_1R distribution and aging as well as sleep deprivation was established [57, 58]. Additional studies on receptor occupancy using PET tracers, for example

[^{18}F]CPFPX in a bolus-plus-constant-infusion PET assay, showed that repeated intake of caffeinated beverages resulted in a 50% occupancy of the cerebral A_1Rs during the day [59]. This effect might cause adaptive changes and lead to chronic alterations of receptor expression and availability. Furthermore, these PET tracers have been valuable tools for clinical studies on neurodegenerative diseases, revealing the functional mechanisms and pharmacokinetic profiles of new potential drug treatment strategies. In early Parkinson's disease, increased binding of [^{11}C]MPDX was found in the temporal lobe, suggesting a compensatory mechanism of A1R expression in non-dopaminergic systems in response to the diminished availability of dopamine [60]. With [^{18}F]CPFPX a phase-and region-specific change pattern of A_1R expression in Huntington's disease was detected, providing evidence that adenosinergic targets are involved in the pathophysiology of this disease [61]. More recently, the first partial agonist PET tracer, [^{11}C]MMPD (Fig. 2, Table 2), was evaluated in rat brain [62]. It showed suitable blood–brain barrier (BBB) permeability, high specificity and subtype selectivity *in vivo*. This finding may open new routes to visualize receptor occupancy of agonists or partial agonists for the A_1R in drug development.

3.2. PET/SPECT tracers for the adenosine A_{2A} receptor

Several radioligands for PET imaging of cerebral A_{2A}Rs have been introduced since the 1990s. The initial design of PET tracers for the A_{2A}R started from xanthine-based antagonists, leading to the discovery of [^{11}C]TMSX (Fig. 2, Table 2), previously abbreviated as [^{11}C]KF18446. Though *in vivo* imaging of the human brain in healthy controls and in patients with Parkinson's disease (PD) was relatively successful [63, 64], these xanthine derivatives are prone to photoisomerization, and thus [^{11}C]TMSX could only be applied in PET scans under dimmed light. To circumvent this limitation, the first non-xanthine-based PET tracer, [^{11}C]SCH442416 (Fig. 2, Table 2), was designed based on a known precursor, SCH58261. An increased binding potential of [^{11}C]SCH442416 was observed in the striatum of Parkinson's patients with levodopa-induced dyskinesias (LIDs), providing evidence that A_{2A}R is a potential pharmacological target for the management of LIDs [65]. Since the problem of high non-specific binding (and consequential low target-to-non-target ratios) still remains for these ligands [66], Zhou *et al*. incorporated the ^{11}C-radionuclide into clinical candidate preladenant. PET imaging in rats showed a high uptake of [^{11}C]preladenant (Fig. 2, Table 2) in the striatum and low uptake in other regions of the brain, consistent with cerebral A_{2A} distribution [67]. Using [^{11}C]preladenant in clinical PET-studies, receptor occupancy by istradefylline, an approved A_{2A}R antagonist, was measured in patients with Parkinson's disease. It was demonstrated that istradefylline binds to A_{2A}R in a dose-dependent manner, consequently

resulting in near-maximal (93.5%) occupancy in the ventral striatum, thus establishing the dosage regimen of such CNS drugs [68]. Subsequently, to extend the half-life of these tracers, ^{18}F-labeled $A_{2A}R$ antagonist PET tracers have been investigated for human studies. For example, two fluorine-18 labeled SCH442416 analogs, [^{18}F]FESCH (Fig. 2, Table 2) and [^{18}F]FPSCH (Fig. 2, Table 2), were reported as PET tracers used to image the $A_{2A}R$ in rat brain [69]. [^{18}F]FESCH and [^{18}F]FPSCH showed identical striatum-to-cerebellum ratios (4.6 at 37 min and 25 min post injection, respectively), similar to the ratio obtained with [^{11}C]SCH442416. Other examples are preladenant-based ligands, including a SPECT tracer, [^{123}I]MNI-420 (Fig. 2, Table 2) and a PET ligand, [^{18}F]MNI-444 (Fig. 2, Table 2). Both have been successfully applied in $A_{2A}R$-imaging studies in the human brain [70, 71]. [^{123}I]MNI-420 rapidly entered the human brain and showed the highest specific binding in the striatum, consistent with known $A_{2A}R$ densities. [^{18}F]MNI-444 showed an improved binding potential in the brain compared to [^{11}C]TMSX and [^{11}C]SCH442416, opening up the possibility to more broadly use *in vivo* A_{2A} PET imaging in neuroscience research.

3.3. PET tracers for the adenosine A_{2B} receptor

So far only two radioligands for use in *in vivo* studies have been developed for $A_{2B}R$, namely 1-[^{11}C]"4" (Fig. 2, Table 2) and -[^{18}F]"7a" (Fig. 2, Table 2) [72] [73]. The first compound, featuring a triazinobenzimidazole scaffold with moderate potency (IC_{50} = 210.2 ± 12.3 nM) toward $A_{2B}R$, has been applied in PET studies in rats and showed the highest uptake in brown adipose tissue, lungs and testes [72]. With a high chemical stability and good pharmacokinetic profile, this tool compound represented a good lead for the development of $A_{2B}R$ radiotracers. The second $A_{2B}R$ PET tracer was developed on a pyrazine-based antagonist with the potential to penetrate the blood-brain barrier [73]. Despite poor selectivity (A_{2A}/A_{2B}=13, A_1/A_{2B}=5) this radiolabeled ligand was further evaluated for its *in vivo* pharmacokinetic profile, revealing the formation of a radio-metabolite capable of penetrating the blood-brain barrier. With these PET studies the stage is set for further $A_{2B}R$ probe design to enhance the selectivity and metabolic stability.

3.4. PET tracers for the adenosine A_3 receptor

The first PET tracer for A_3R was developed by radiofluorination FE@SUPPY (Fig. 2, Table 2), a selective and potent antagonist for hA_3R [74, 75]. Though it had already been shown for the parent compound that the affinity for rat A_3R was 140 fold lower than for human A_3R, [^{18}F]FE@SUPPY was studied for its biodistribution in rats and specific binding in the rat brain was demonstrated using autoradiography [76]. A further preclinical PET study using

[^{18}F]FE@SUPPY to image A_3R revealed a pronounced uptake in xenografted mice injected with cells overexpressing human A_3R. This "humanized animal model" inspired to evaluate [^{18}F]FE@SUPPY in mice xenografted with a human colorectal cancer cell line (HT-29) overexpressing A_3R as a tumor marker. Unfortunately, this study to visualize the A_3R *in vivo* was unsuccessful, presumably due to insufficient uptake of [^{18}F]FE@SUPPY in the tumors, poor conservation of target expression in xenografts or unfavorable pharmacokinetics of the tracer in mice [77]. In analogy to this, [^{18}F]FE@SUPPY:2 (Fig. 2, Table 2) was developed by transforming the fluoroethylester into a fluoroethylthioester [78]. While a higher specific radioactivity was obtained ([^{18}F]FE@SUPPY:2 = 340 ± 140 GBq/mol and [^{18}F]FE@SUPPY = 70 ± 26 GBq/mol), the uptake pattern for the two PET tracers is distinct. Especially brain to blood ratios are remarkably increased over time for [^{18}F]FE@SUPPY whereas those for [^{18}F]FE@SUPPY:2 stayed unaltered. Lastly, a pair of structurally similar ligands (i.e. agonist MRS3581 and antagonist MRS5147) were reported as [^{76}Br]-labeled potential PET radiotracers [79]. Both ligands showed similar biodistribution in rats: primarily uptake in the organs of metabolism and excretion. However, the uptake of agonist [^{76}Br]MRS3581 (Fig. 2, Table 2) was an order of magnitude faster than that of antagonist [^{76}Br]MRS5147 (Fig. 2, Table 2), possibly due to the presence of a uronamide group in the agonist to influence its bioavailability and permeation *in vivo*. In contrast, the antagonist [^{76}Br]MRS5147 demonstrated an increased uptake in rat testes, an A_3R-rich tissue, suggesting that the antagonist may also serve as a viable diagnostic molecular probe for pathological conditions with increased A_3R expression.

Table 2 Recent AR radioligands used for clinical PET or SPECT imaging

	Radioligands	K_D (nM)[a]				Functionality	Ref
		A_1	A_{2A}	A_{2B}	A_3		
A_1							
	[^{18}F]CPFPX	1.26	940	N.D.	N.D.	Antagonist	[51]
	[^{11}C]MPDX	4.2 (r)	>100 (r)	N.D.	N.D.	Antagonist	[51]
	[^{11}C]MMPD	0.5	71	75	42 % (1 μM)	Partial Agonist	[62]
A_{2A}							
	[^{11}C]TMSX or [^{11}C]KF18446	1600 (r)	5.9 (r)	N.D.	N.D.	Antagonist	[80]
	[^{11}C]SCH442416	1.11	0.05	>10,000	>10,000	Antagonist	[81]
	[^{11}C]preladenant	>1000	1.1	>1700	>1000	Antagonist	[82]
	[^{18}F]FESCH	42.7% (10 μM)	12.4	N.D.	59.6% (10 μM)	Antagonist	[83]
	[^{18}F]FPSCH	1000	53.6	N.D.	1320	Antagonist	[84]
	[^{18}F]MNI-444	N.D.	2.8	N.D.	N.D.	Antagonist	[85]
	[^{123}I]MNI-420	N.D.	2.0	N.D.	N.D.	Antagonist	[85]
A_{2B}							
	[^{11}C]"4"	230.3	548.0	210.2	N.A.	Antagonist	[72]
	[^{18}F]"7a"	19.0	55.0	4.24	796	Antagonist	[73]
A_3							
	[^{18}F]FE@SUPPY	4030	1720	N.D.	6.02	Antagonist	[77]
	[^{76}Br]MRS3581	N.D.	N.D.	N.D.	0.63	Agonist	[79]
	[^{76}Br]MRS5147	N.D.	N.D.	N.D.	0.62	Antagonist	[79]

[a] The data are K_D-values of radiolabeled compounds for human adenosine receptors unless otherwise indicated (r= rat) or % inhibition at the indicated concentration in bracket. N.D. = not determined, N.A. = not active

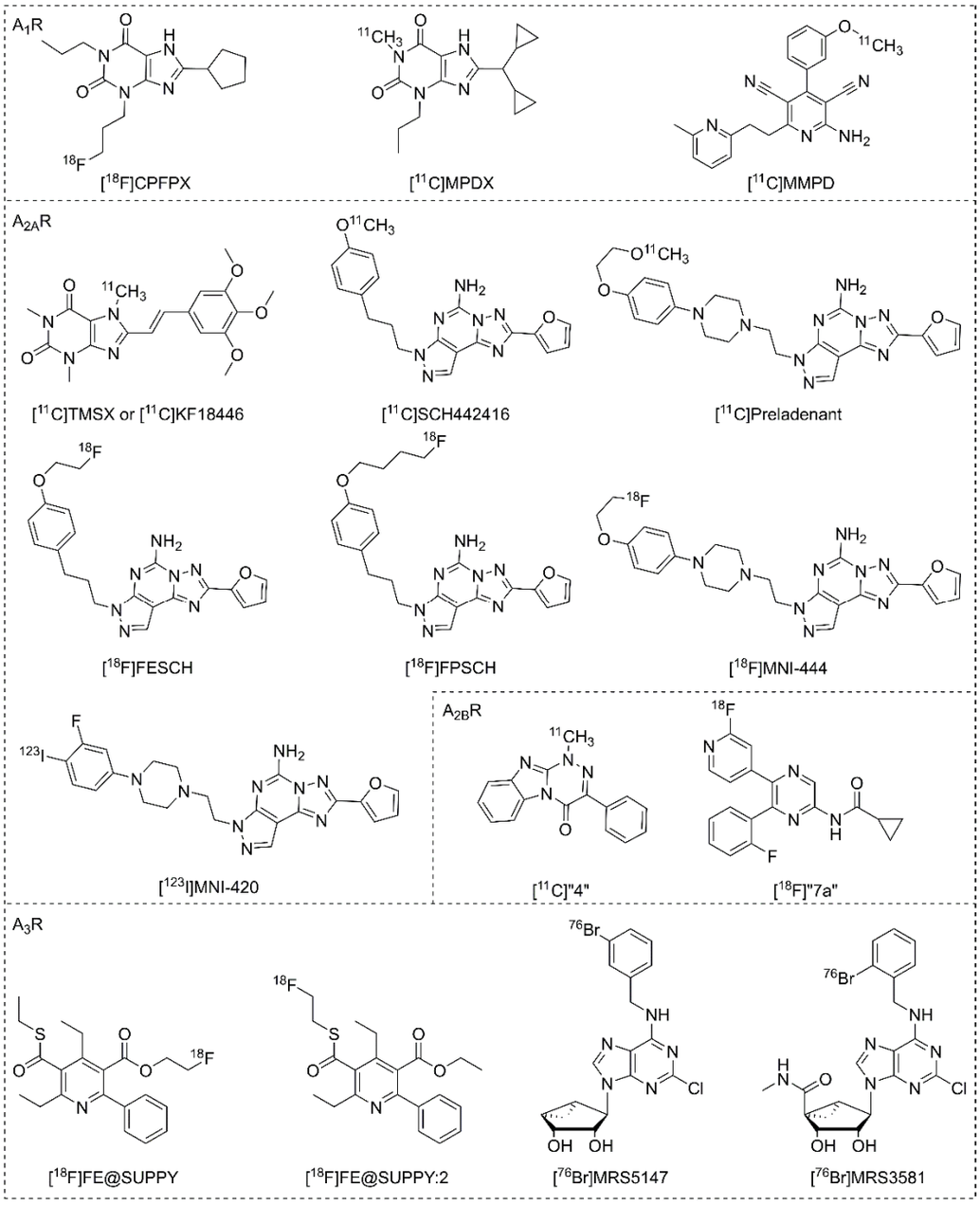

Fig. 2 Chemical structures of AR radioligand tracers for *in vivo* studies

4. Fluorescent probes

As an alternative to radiolabeled molecular probes, fluorescent ligands have also been included into the pharmacological toolbox. This approach avoids the safety concerns associated with the disposal of radioisotopes and also provides the opportunity of a "real-time" readout of the ligand-receptor interaction. Fluorescent ligands for GPCRs are usually designed by incorporating a relatively small organic fluorophore, such as a BODIPY-, Alexa Fluor-, rhodamine-, or NBD (nitrobenzoxadiazole) moiety into an existing GPCR agonist or antagonist pharmacophore via a linker. The use of these fluorescent probes can provide more insight in receptor localization, function and regulation, but also onligand-target binding kinetics, thus contributing to a detailed understanding of receptor physiology and pathophysiology. In addition, the development of newer fluorescent methods and techniques, such as scanning confocal microscopy (SCM), fluorescence polarization (FP), fluorescence correlation spectroscopy (FCS), resonance energy transfer (FRET or BRET) and flow cytometry (FCM), are boosting the potential use of fluorescent probes in drug discovery. The development of fluorescent ligands to characterize adenosine receptors has been the subject of intense investigation, which has been summarized in detail by Kozma *et al.* in 2013 [86]. Here we will therefore summarize and review emerging fluorescent ligands for more recent applications on ARs.

4.1. Fluorescent ligands for the adenosine A_1 receptor

To monitor ligand binding to receptors on the surface of living cells, a Nano-luciferase (NanoLuc) BRET methodology (NanoBRET) has recently been established [87-89]. This approach was also applied to a study of allosteric modulators in intact living cells using fluorescent A_1R agonists, such as the adenosine-based agonist, ABA-X-BY630 (Fig. 3, Table 5), and two NECA-based ligands, ABEA-X-BY630 (Fig. 3, Table 5) and BY630-X-(D)-A-(D)-A-G-ABEA (Fig. 3, Table 5) [90]. The two positive allosteric modulators tested were shown to increase the specific binding of the fluorescent A_1R agonists, indicative for a switch of the A_1R population to a more active receptor conformation.

4.2. Fluorescent ligands for the adenosine A_{2A} receptor

MRS5424 (Fig. 3, Table 5) is a fluorescent adduct of agonist APEC with Alexa Fluor 532. Using this probe, allosteric modulation within $A_{2A}R/D_2R$ heterodimers was followed using real-time FRET [91]. A negative allosteric effect on $A_{2A}R$ ligand binding and receptor activation was found when the D_2R agonist quinpirole was added. This heterodimer interaction was further validated in a higher-throughput flow cytometry-based assay with the

fluorescent agonist MRS5206 (APEC-Alexa Fluor 488) (Fig. 3, Table 5) [92]. These experiments provided evidence for a differential D_2R-mediated negative allosteric modulation of $A_{2A}R$ agonist binding, in particular for apomorphine, a drug used in the treatment of PD. Recently, using a fluorescence polarization assay, McNeely *et al*. employed a fluorescent agonist, FITC-APEC (Fig. 3, Table 5), to characterize the binding kinetics of three $hA_{2A}R$ ligands [93, 94]. The kinetic parameters of these unlabeled ligands, computed using a numerical solution approach, showed good consistency with those determined in a conventional radioligand binding assay.

Endeavors to enhance selectivity towards $hA_{2A}R$ and improve the physicochemical properties of fluorescent ligands led to the discovery of MRS7416 (Fig. 3, Table 5), which is based on the antagonist SCH442416 [95]. As a fluorescent tracer, MRS7416 displayed low nonspecific binding at $hA_{2A}R$ in flow cytometry experiments. From molecular docking studies the researchers suggested that the fluorescent AlexaFluor488 moiety present in MRS7416 is binding to the hydrophilic extracellular loops of the receptor. This would make the probe essentially 'bitopic', i.e. bridging two separate domains of the $hA_{2A}R$.

4.3. Fluorescent ligands for the adenosine A_{2B} receptor

The first selective A_{2B} fluorescent ligand reported, PSB-12105 (Fig. 3, Table 5), was synthesized by integrating a BODIPY moiety into the pharmacophore of 8-substituted xanthine derivatives [96]. Besides fluorescently labeling CHO cells expressing recombinant human $A_{2B}R$, this ligand was used to establish an $A_{2B}R$ binding assay on living cells in a flow cytometry set-up. Barresi *et al.* reported on another series of (non-selective) fluorescent antagonists for labeling A_1Rs and $A_{2B}Rs$ [97]. In one of the ligands a fluorescent group, 7-nitrobenzofurazan group (NBD) (Fig. 3, Table 5), was linked to a triazinobenzimidazole scaffold. This fluorescent antagonist showed a clear labeling of bone marrow-derived mesenchymal stem cell membranes, which was largely prevented by pre-incubation with selective agonists for A_1R and $A_{2B}R$. These findings provide an important basis for the design of novel fluorescent ligands to monitor the expression and localization of $A_{2B}R$ in living cells.

4.4. Fluorescent ligands for the adenosine A_3 receptor

The non-selective A_1R/A_3R antagonist, CA200645, was employed as a tool compound to develop a robust competition binding assay to e.g., screen for new chemical templates and fragments for A_3R at a live cell high content screening system [87, 88]. Besides, CA200645 was also applied to study the A_3R localization on intact human neutrophils. It appeared that A_3R activation induces the formation of filipodia-like extensions and bacterial phagocytosis

[98]. Modification of the linker component in CA200645 by the insertion of a dipeptide yielded two A_3-selective fluorescent ligands, BODIPY 630/650-X-Tyr-Ser-XAC (Fig. 3, Table 5) and BODIPY FL-X-Tyr-Ser-XAC (Fig. 3, Table 5) [99]. Both ligands showed displaceable membrane binding with little non-specific binding in a fluorescent confocal microscopy set-up.

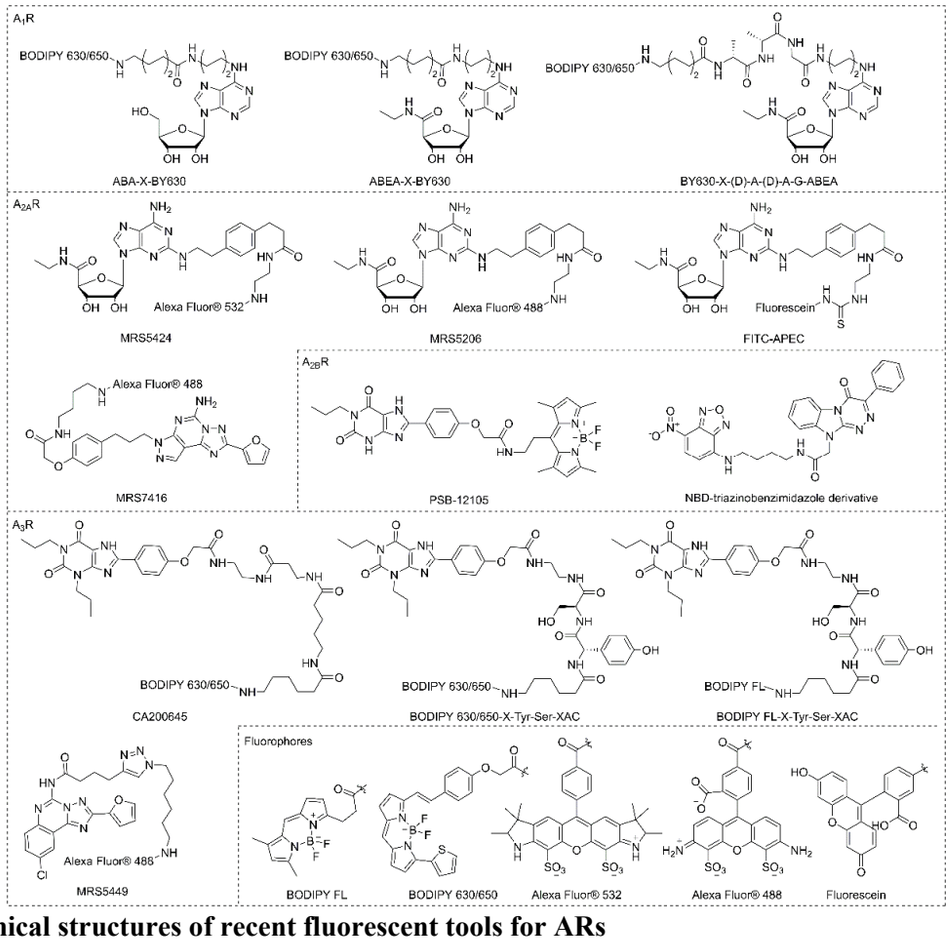

Fig. 3 Chemical structures of recent fluorescent tools for ARs

A similar strategy to incorporate a (three amino acid) peptide linker was applied to an existing non-selective adenosine-based fluorescent agonist, ABEA-X-BY630, yielding the highly potent fluorescent agonist BY630-X-(*D*)-Ala-(*D*)-Ala-Gly-ABEA at A_3R [100]. This probe was used to visualize the internalization of YFP-tagged as well as untagged receptors, and appeared to promote the formation of intracellular receptor-arrestin3 complexes. In addition, click chemistry serves as a versatile approach to simplify compound synthesis, as it provides the means for facile incorporation of fluorescent tags. CGS15943, a triazolo-quinazoline antagonist scaffold, was extended with an alkyne moiety to be click-conjugated with Alexa Fluor-488, yielding a selective A_3R fluorescent probe, MRS5449 (Fig. 3, Table 5) [101]. In

flow cytometry this molecular probe was used to quantify hA_3R and to perform ligand screening in intact cells.

Table 3 Recent AR fluorescent ligands

Ligands	pK_D[a]				Functionality	Ref
	A_1	A_{2A}	A_{2B}	A_3		
A_1						
CA200645	7.47 ± 0.34	N.D.	N.D.	8.21 ± 0.12	Antagonist	[87, 89]
ABA-X-BY630	6.23 ± 0.05	N.D.	N.D.	N.D.	Agonist	[90]
ABEA-X-BY630	5.99 ± 0.15	N.D.	N.D.	N.D.	Agonist	[90]
BY630-X-AAG-ABEA	6.17 ± 0.16	N.D.	N.D.	N.D.	Agonist	[90]
A_{2A}						
FITC- APEC	N.D.	57[c]	N.D.	N.D.	Agonist	[93, 94]
MRS7416	1680[b]	30.3[b]	N.D.	32 ± 3%[b] (10 µM)	Antagonist	[95]
A_{2B}						
PSB-12105	≥10 000[b]	>10 000[b]	1.83[b]	>10 000[b]	Antagonist	[96]
NBD-derivative	1380[b]	>10 000[b]	20.7 ± 7.5 %[c]	>10 000[b]	Antagonist	[97]
A_3						
BODIPY 630/650-X-Tyr-Ser-XAC	7.62 ± 0.13[d]	N.D.	N.D.	9.12 ± 0.05	Antagonist	[99]
BODIPY FL-X-Tyr-Ser-XAC	6.50 ± 0.04[d]	N.D.	N.D.	7.96 ± 0.09	Antagonist	[99]
MRS5449	87.0[b]	73.0[b]	N.D.	6.4[b]	Antagonist	[101]

[a] The data are pK_D-values for compounds for the indicated human adenosine receptors. N.D. = not determined

[a] K_D-value at the bovine adenosine A_{2A} receptor

[b] Data are K_i-values of compounds (nM) for the indicated human adenosine receptors or % displacement at the indicated concentration in brackets.

[c] cAMP production in CHO cells expressing human $A_{2B}R$ at the concentration of 10 nM compound in the presence of 100 nM of NECA. Data are expressed as percentage of cAMP production versus agonist maximal effect (100%).

[d] Data are pKi-values for human A_1R from radioligand binding assay.

5. Covalent ligands

Another class of molecular probes is formed by covalent ligands. The term covalent here refers to the ability of these compounds to bind the receptor irreversibly by forming a covalent bond to a specific amino acid residue located at or near the ligand binding site [102]. Some different considerations can be made depending on the type of covalent interaction induced. Generally, high affinity and selectivity for the target receptor will increase receptor occupancy

and decrease non-specific or off-target binding, thus improving specific covalent labeling [103]. Two types of covalent ligands have been developed until now: electrophilic and photoreactive ligands. Choosing the correct functional group (or warhead) that can react with the amino acid residues present in the binding site is essential for successful molecular probe design. Photoreactive ligands possess a light-sensitive group, such as aryl azide, diazirine or benzophenone, which can be irradiated with light of a specific wavelength to yield highly reactive nitrene, carbene or benzophenone-derived diradicals. These reactive species can subsequently form a covalent bond with a neighboring amino acid residue through a variety of insertion reactions [104]. Photoreactive ligands, occasionally combined with mass spectometry, have been applied in GPCR research to determine the binding site of ligands and to identify the partner-receptor for orphan ligands [105]. When combined with a radioactive label, photoaffinity probes emerge, which can be used to study GPCR localization using autoradiography [106]. Electrophilic ligands on the other hand possess a reactive electrophile as a warhead, such as (iso)thiocynate, sulfonyl fluoride or a Michael acceptor like acrylamide. These electrophiles react with nucleophilic amino acid residues such as lysine, serine and cysteine near the binding site of the ligand. When combined with *in silico* modeling and site-directed mutagenesis studies, these chemo-reactive ligands often enable characterization of the GPCR-ligand binding site. Additionally, electrophilic covalent ligands have been applied to study receptor reserve, turnover and subtype discrimination [107, 108]. Lastly, binding of a covalent ligand stabilizes the receptor into an active or inactive conformation, which in turn facilitates crystallization of the receptor-ligand complex. This aids in crystallization studies using X-ray or cryoEM, providing valuable insights into the structure and function of GPCRs [109]. A prime example of this is the case of the human adenosine A_1 receptor which was recently co-crystallized with covalent antagonist DU172 [3]. There are numerous reported covalent ligands for adenosine receptors that have in some way contributed to the characterization of these receptors and their ligand binding sites. These ligands will be summarized below and their applications will be discussed.

5.1. Covalent ligands for the adenosine A_1 receptor

Arguably the first example of photoaffinity labeling of an adenosine receptor dates back to 1985 when N^6-2-(4-aminophenyl)ethyladenosine (APNEA), a nonselective adenosine-based agonist with high affinity for both A_1R and A_3R, was coupled to the A_1R [110]. In an attempt to characterize the A_1R structure, radioiodinated [^{125}I]APNEA (Fig. 4, Table 4) was incubated with A_1R and reacted with crosslinking reagent *N*-hydroxysuccinimidyl 6-(4-Azido-2-nitrophenylamino)hexanoate (SANPAH) *in situ* . Subsequent UV-irradiation resulted in a 38

kDa protein being covalently labeled with the radioligand in rat cerebral cortex and adipocyte membranes. Since this process was completely blocked by co-incubating with a selective A_1R agonist, this protein was designated as A_1R. Strictly speaking, this radioactive ligand is obviously not inherently photo-reactive and thus not a photoaffinity probe *per se*. Interestingly, in the same year efforts to develop an inherently photoreactive ligand based on the *R*-PIA scaffold, one of the most selective A_1R agonists, were successful. A photoactivatable azido group was positioned at the purine core structure, generating the photolabile ligand *R*-AHPIA (Fig. 4, Table 4) [111]. It exhibited similar affinity (K_i = 1.5 nM) and efficacy (EC_{50} = 35 nM) as its parent compound, *R*-PIA, but after photoactivation it showed irreversible inhibition of approximately 40% of the receptor binding sites. Such covalent labeling of A_1R led to a concentration-dependent reduction of cellular cAMP levels, consistent with activation of rA_1R and correlating with receptor occupancy [112]. Similar to the case of APNEA, when *R*-AHPIA was radioiodinated to yield [^{125}I]AHPIA (Fig. 4, Table 4), SDS-PAGE analysis of rat brain membranes that were incubated with this covalent radioligand and UV-irradiated, showed the appearance of a single protein band of ~35 kDa [111]. Interestingly, even though *R*-AHPIA is about 60-fold selective for the A_1R, it is also a partial agonist at the $A_{2A}R$, and pretreatment with *R*-AHPIA reduced the stimulatory effect of NECA, indicating persistent binding of the ligand and subsequent reduced activation by a full agonist. [113]. In the search for covalent antagonists, 4-azidophenethyl xanthine derivative [^{125}I]BW-A947U (Fig. 4) was synthesized and optimization (analogous to the development of selective A_1R antagonist DPCPX) gave the next photoactivatable antagonist, [^{125}I]azido-BW-A844U (Fig. 4, Table 4) [114-116]. Both ligands are xanthine-based antagonists that have a light-sensitive aryl azide located on the xanthine 3-position. Photoaffinity labeling of partially purified receptor with [^{125}I]azido-BW-A844U followed by chemical or enzymatic fragmentation experiments demonstrated that the covalently modified amino acids were located at transmembrane domain III of the A_1R. This approach provided clear insight into the amino acids surrounding the binding pocket of the A_1R and thus aided in the development of three-dimensional models of the receptor.

Initial attempts in the development of chemo-reactive agonist ligands for the A_1R were focused on functionalizing the adenosine scaffold with isothiocyanates or sulfonyl fluorides to serve as warheads [117, 118]. In the first reported case, *p*- and *m*-DITC-ADAC (Fig. 4, Table 4), both adenosine derivatives with nanomolar affinity substituted on the N^6-position with an isothiocyanate-bearing linker, were synthesized and tested on the A_1R [119]. At nanomolar

concentration both ligands irreversibly occupied approx. half of the A_1R binding sites. In a functional cAMP accumulation assay both agonists elicited a sustained, antagonist-insensitive, A_1R-mediated response. Since the incorporation of a warhead via the N^6-position of the adenosine scaffold was well tolerated and showed no negative effect on the ligands' affinities, a series of adenosine derivatives bearing diverse linker types and warheads were synthesized and examined. Two promising compounds, isothiocyanate **15b** and sulfonyl fluoride **15d** (Fig. 4, Table 4), were validated as irreversible agonists promoting persistent A_1R-mediated guanine nucleotide exchange activity in a manner resistant to both agonist and antagonist addition [118]. Furthermore, these two ligands demonstrated their capacity to thermo-stabilize purified, detergent-solubilized A_1R in a ThermoFluor assay to a significantly higher degree than the high affinity agonist NECA could. These thermostabilized receptors with covalently bound ligands allowed purification of the receptor in a monodisperse state, which greatly facilitated structure determination by X-ray crystallography [118].

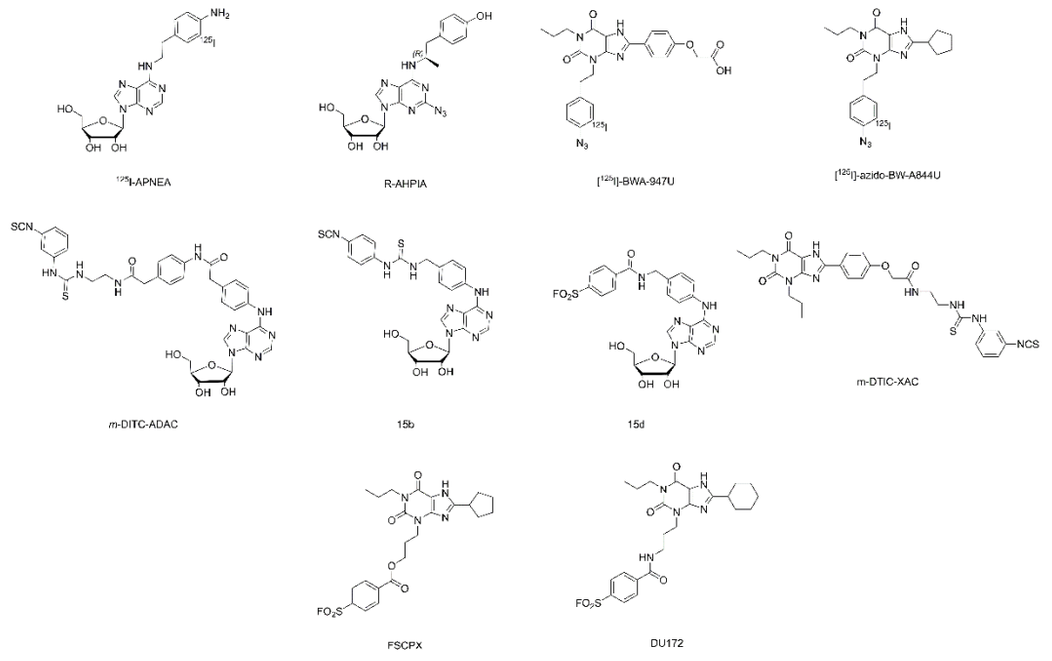

Fig. 4 Chemical structures of covalent ligands for A_1R

With respect to chemo-reactive antagonists two approaches have been explored, both starting from the xanthine scaffold. The first class comprises the 8-substituted 1, 3-dipropylxanthines [117]. One such compound is *m*-DITC-XAC (Fig. 4, Table 4), an isothiocyanate derivative of the relatively non-selective AR antagonist XAC. It was found to be a potent A_1R antagonist in rat brain (K_i = 2.39 ± 0.35 nM), and was used to study the receptor reserve in guinea pig atrioventricular nodes [120]. In the second approach the electrophilic fluorosulfonyl group

was placed on the 3-position of the xanthine core, as was done in covalent tool FSCPX (Fig. 4, Table 4) [121]. This compound had a good affinity for the A_1R (IC_{50} = 10 ± 3 nM) and treatment with 10 or 50 nM FSCPX led to reductions in the available A_1R binding sites of 60% and 74%, respectively. In a follow-up study it demonstrated that FSCPX irreversibly antagonized cardiac A_1R-mediated responses. Subsequently it was shown that FSCPX was unable to significantly decrease the maximal direct inotropic response to four A_1R full agonists (NECA, CPA, CHA and adenosine) in guinea pig atria, which demonstrated a considerable A_1R reserve for direct negative inotropy [122]. In *in vivo* experiments, FSCPX was used successfully as a "receptor knock-down" tool when IV-infusion of FSCPX in conscious rats attenuated CPA-mediated bradycardia [123]. As the ester bond present near the warhead of FSCPX is prone to hydrolysis, a follow-up structural modification was performed with a focus on linker types [124, 125]. This resulted in a closely related analog with improved stability, DU172 (Fig. 4, Table 4). The affinity of DU172 (IC_{50} = 24.9 ± 7.6 nM) was in line with that of FSCPX and pretreatment of DDT_1 MF2 cells with DU172 resulted in a concentration-dependent decrease in the A_1R binding sites, indicating that it behaved as an irreversible ligand indeed. This covalent ligand-receptor interaction has been the basis for the structure elucidation of A_1R due to improved receptor stability [3].

5.2. Covalent ligands for the adenosine A_{2A} receptor

For the $A_{2A}R$ initial characterization of the receptor was aided by a radio-iodinated analog of APEC, a prototypical ribose-based selective $A_{2A}R$ agonist. Similar to the initial A_1R studies, [^{125}I]PAPA-APEC (Fig. 5, Table 4) was cross-linked to the $A_{2A}R$ in bovine striatal membranes using SANPAH and was shown to covalently label a 45-kDa protein [126, 127]. Both NECA and R-PIA were able to prevent the covalent labeling of the 45-kDa protein by [^{125}I]PAPA-APEC, providing evidence that this protein is the $A_{2A}R$ indeed. Subsequently, the photoactivatable azido analog [^{125}I]azido-PAPA-APEC (Fig. 5, Table 4) was developed and was used to directly label the same 45-kDa protein in bovine striatal membranes with 3-fold greater efficiency of photo-incorporation [128]. A further characterization of the binding domain was performed by Piersen *et al.*, who performed photoaffinity labeling of the canine $A_{2A}R$ overexpressed in COS M6 cells with [^{125}I]azido-PAPA-APEC and tracked the cross-linked transmembrane domain V [129]. However, no individual amino acid residues responsible for the covalent interaction were identified. These studies were later repeated with a novel adenosine-based radioligand [^{125}I]APE, which showed less hydrophobic interactions than [^{125}I]PAPA-APEC and had higher specific radioactivity than [^{3}H]CGS21680 [130]. Its azido analog, [^{125}I]AzPE (Fig. 5, Table 4), showed saturable, high-affinity binding in rabbit

striatal membranes (K_D = 1.7 ± 0.5 nM), and photolabeling identified a protein of 45 kDa that displayed the appropriate pharmacology of the $A_{2A}R$. More recently, photoaffinity labeling is often combined with mass spectrometry analysis to map detailed ligand-receptor binding sites. Muranaka *et al.* incorporated the trifluoromethyl diazirine group into a not-so-$A_{2A}R$-selective SCH58261 analogue to give photoaffinity ligand NUMBER 9 (Fig. 5, Table 4) [131-133]. When purified $hA_{2A}R$ was photolabeled with this ligand and subjected to protease digestion, cross-link positions were identified with LC-MS/MS. The most likely amino acid candidate for this ligand was $Y271^{7.36}$ in transmembrane domain VII. This is the first reported case in which the cross-linked amino acid was elucidated by mass spectrometry, which demonstrates the power of combining mass spectrometry–based proteomics and covalent labeling in the elucidation and characterization of GPCR ligand binding sites.

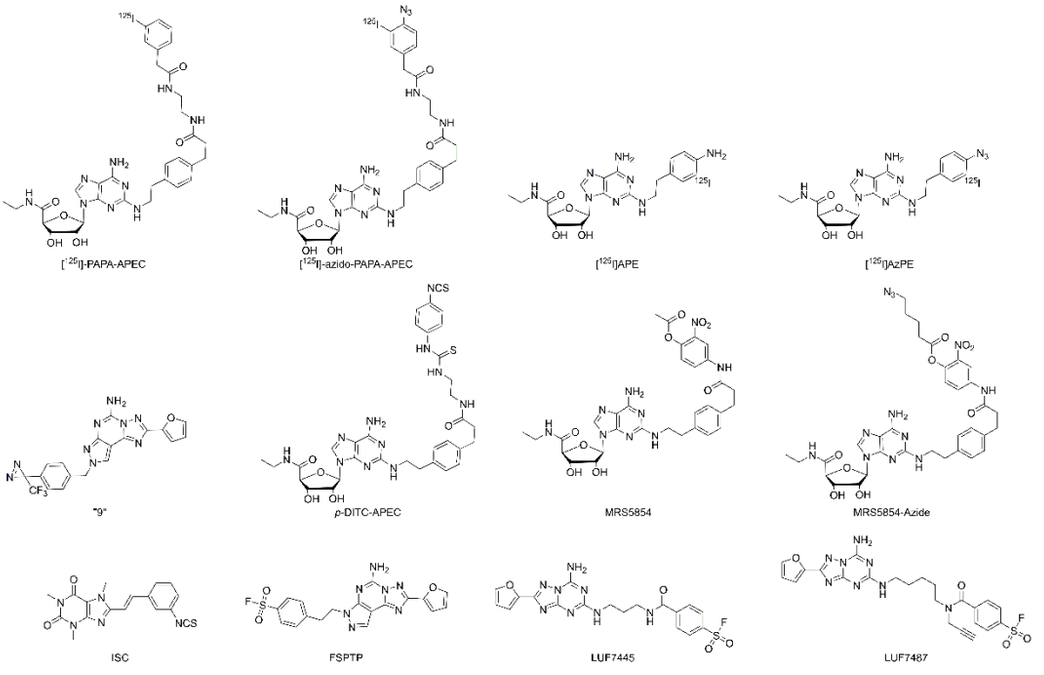

Fig. 5 Chemical structures of covalent ligands for $A_{2A}R$

Analogous to the photo-reactive ligands, APEC also served as a parent ligand for the initial design of chemo-reactive ligands for $A_{2A}R$. One exemplary compound is *p*-DITC-APEC (Fig. 5, Table 4), which has a reactive 4-isothiocyanatophenyl residue attached to the C-2 substituent of the purine ring [127]. It had good affinity (K_i = 7.1 ± 2.3 nM at bovine $A_{2A}R$) [127] and, at a concentration of 100 nM, irreversibly blocked 77% of [^{3}H]CGS21680 binding in rabbit striatal membranes [134]. In isolated, perfused guinea pig hearts treatment with *p*-DITC-APEC caused a prolonged, persistent, and concentration-dependent coronary vasodilatation, which is evidence of an irreversible activation of $A_{2A}R$ [135]. More recently,

an APEC-analogue bearing an active 2-nitrophenyl ester was synthesized (MRS5854, Fig. 5, Table 4). This ligand was designed to bind to the receptor irreversibly and subsequently transfer its terminal acyl group to a nucleophilic amino acid residue on extracellular loop 2 (ECL2) of the $A_{2A}R$ [136]. This acyl transfer would prevent the ECL2-lysine-mediated recognition of ligands, effectively blocking the receptor. Preincubation of $hA_{2A}R$ with MRS5854 followed by extensive washing indeed showed near-complete inhibition of radioligand binding. When ECL2-lysine K153 was mutated to an alanine residue, a partial restoration of B_{max} was observed after treatment with MRS5854, confirming that K153 is the anchor point for the covalent interaction. Interestingly, the K_D for the radioligand used ([^{3}H]ZM241385) was not significantly influenced by this mutation, indicating that the targeted lysine residue is not important for ligand binding and that acyl transfer seems to prevent binding by blocking entry to the binding pocket instead of preventing the recognition of ligands. In parallel, the active acyl was replaced by an azido-pentanoate group to generate MRS5854-azide. Though this ligand showed diminished affinity towards the $A_{2A}R$, it nevertheless showed a slight reduction in B_{max}, suggesting that at least part of the receptors were covalently labeled with the azido-pentanoate. This azido-group could allow for click-ligation to functionalized alkynes; however, biologic data has not yet been reported.

Three approaches have been taken to develop electrophilic covalent probes for the $A_{2A}R$. The first example is ISC (Fig. 5, Table 4), an isothiocyanate-functionalized xanthine-based antagonist for $A_{2A}R$, which irreversibly binds to 80% of $rA_{2A}R$ at 20 μM [137]. A second approach yielded FSPTP (Fig. 5, Table 4), the *para*-fluorosulfonyl derivative of SCH58261, which was used to investigate the level of $A_{2A}R$ reserve [138]. More recently, our research group used the molecular structure of the antagonist ZM241385 as a starting point for the design of a third electrophilic covalent ligand. This endeavor yielded LUF7445 (Fig. 5, Table 4), a potent fluorosulfonyl-equipped antagonist with an apparent affinity for the $hA_{2A}R$ in the nanomolar range (pK_i = 8.99 ± 0.008) [139]. Aided by site-directed mutagenesis studies, it was shown that LUF7445 binds to $K153^{ECL2}$, the same residue that was also involved in the acyl transfer of covalent agonist MRS5854. After optimization of the chemical structure, the most potent ligandwas retained for further structural modification and was equipped with an alkyne click handle (next to the warhead), resulting in the bifunctional probe LUF7487 (Fig. 5, Table 4) [6]. This affinity-based probe made it possible to visualize the receptor on SDS-PAGE via click-ligation with a sulfonated Cy-3 fluorophore. The $hA_{2A}R$ was successfully labeled in cell membranes, making LUF7487 a promising tool compound that sets the stage

for the further development of probes to study GPCRs. The development of affinity-based probes may open the door for the identification and target validation of GPCRs in a more native environment.

5.3. Covalent ligands for the adenosine A_3 receptor

While there are no photo-reactive or chemo-reactive ligands available for the $A_{2B}R$ (i.e. the so far least studied AR in general), the case for the A_3R is also still rather minimal. No photo-reactive ligands and only four "classes" of chemo-reactive ligands are available for the A_3R. MRS1163 (Fig. 6, Table 4), the only irreversibly binding agonist for the A_3R, was derived from the selective A_3R agonist IB-MECA [140]. It features a chemo-reactive isothiocyanate moiety, which replaced the iodine substituent on IB-MECA, and showed an apparent K_i value in the low nanomolar range (10.0 ± 2.3 nM), which is comparable to IB-MECA. Treatment of rA_3R with 100 nM of MRS1163 led to a 41% loss in the available receptor binding sites and its irreversible nature was demonstrated by the lack of recovery of A_3R binding sites after extensive washing.

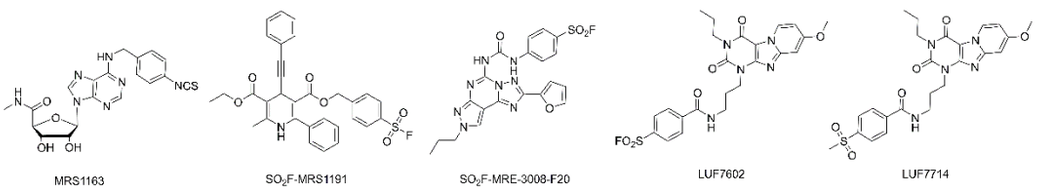

Fig. 6 Chemical structures of covalent ligands for A_3R. Note: LUF7714 is a reversible control ligand for LUF7602.

Using a "functionalized congener approach" the Jacobsen group developed an electrophilic antagonist for the A_3R based on the 1,4-dihydropyridine template, a selective A_3R scaffold. A fluorosulfonyl-substituted phenyl group was installed on MRS1191, thereby generating the functionalized congener SO_2F-MRS1191 (Fig. 6, Table 4) [141]. It was reported to possess greatly improved affinity (2.42 ± 0.32 nM) over the corresponding sulfonamide compound, which displayed moderate potency of only 0.292 ± 0.030 μM. When 100 nM of compound 19 was incubated with hA_3R-transfected HEK-293 cell membranes, approximately 56% of the hA_3R binding sites were irreversibly occupied. A second covalent antagonist was generated based on MRE-3008-F20, a highly potent and selective A_3R antagonist [142]. By replacing the methoxy group in MRE-3008-F20 with a sulfonyl fluoride moiety an irreversibly binding derivative, SO_2F-MRE-3008-F20 (Fig. 6, Table 4), was synthesized. At a concentration of 100 nM, SO_2F-MRE-3008-F20 inhibited binding of the radioligand [^{125}I]AB-MECA by 79%. By docking the ligand in a homology model of the A_3R, it was speculated that two amino

acids, Cys251 or Ser247, are the most probable binding partners for covalent interaction. Recently, our group used a chemical structure-based approach to design covalent antagonists for the hA_3R [143]. A series of tricyclic xanthine-derived ligands bearing a fluorosulfonyl warhead and varying linkers was synthesized. The most potent ligand, LUF7602 (Fig. 6, Table 4) had high affinity for the hA_3R (pK_i = 8.0 ± 0.05). Additionally, a nonreactive methylsulfonyl derivative LUF7714 was developed as a reversible control compound. A series of assays, comprising of time-dependent affinity determination, washout experiments, and [^{35}S] GTPγS binding assays, then validated LUF7602 as a covalent antagonist. Based on homology-docking, tyrosine $Y265^{7.36}$ was identified as potential covalent anchor and when this residue was mutated to phenylalanine the mutant receptor displayed a significant decrease in affinity for LUF7602 (pIC_{50} = 7.8 ± 0.05 for hA_3R-WT, pIC_{50} = 6.0 ± 0.3 for hA_3R-$Y265^{7.36}F$), while the affinity of LUF7714 (pIC_{50} = 5.9 ± 0.2 for hA_3R-WT, pIC_{50} = 6.0 ± 0.1 for hA_3R-$Y265^{7.36}F$) was unaltered. It is worth mentioning that this particular tyrosine residue is conserved amongst adenosine receptors, and is also the anchor point of DU172, the aforementioned covalent antagonist for the hA_1R [124]. Hence, this tyrosine residue potentially represents a universal anchor point for covalent probes designed for adenosine receptors. In general, covalent probes, supported by molecular modeling and site-directed mutagenesis, can serve as powerful tools to characterize the spatial orientation and topography of ligand-receptor binding sites.

Table 4 Covalent ligands for adenosine receptors

Ligands	K_i[a]				Functionality	Ref
	A_1	A_{2A}	A_{2B}	A_3		
A_1						
[^{125}I]APNEA	K_D = 2 nM (r)	N.D.	N.D.	N.D.	Agonist	[110]
R-AHPIA	1.6 nM (r)	N.D.	N.D.	N.D.	Agonist	[110]
[^{125}I]AHPIA	K_D = 2 nM (r)	N.D.	N.D.	N.D.	Agonist	[110]
[^{125}I]azido-BW-A844U	K_D = 0.14 nM (b)	N.D.	N.D.	N.D.	Antagonist	[116]
p- DITC-ADAC	0.469 nM (r)	191 nM (r)	N.D.	N.D.	Agonist	[117]
m-DITC-ADAC	0.867 nM (r)	176 nM (r)	N.D.	N.D.	Agonist	[117]
m-DITC-XAC	2.39 nM (r)	343 nM (r)	N.D.	N.D.	Antagonist	[117]
FSCPX	IC_{50} = 11.8 nM	IC_{50} = 1200 nM	N.D.	N.D.	Antagonist	[124]
DU172	IC_{50} = 21 nM	IC_{50} = 2.8 nM	N.D.	N.D.	Antagonist	[124]
A_{2A}						
[^{125}I]Azido-PAPA-APEC	N.D.	K_D = 1.2 nM	N.D.	N.D.	Agonist	[128]
[^{125}I]AzPE	N.D.	K_D = 1.7 nM	N.D.	N.D.	Agonist	[130]
NUMBER 9	N.D.	39.7 nM	N.D.	N.D.	Agonist	[133]
p-DITC-APEC	276 nM (r)	35 nM (r)	N.D.	N.D.	Agonist	[127]
MRS5854	500 nM	23.0 nM	N.D.	207 nM	Agonist	[136]
MRS5854-azide	30% (10 μM)	4360 nM	N.D.	1810 nM	Agonist	[136]
ISC	20.3 μM	111 nM	N.D.		Antagonist	[137]
LUF7445	372 nM	1.0 nM	0% (1 μM)	49 nM	Antagonist	[139]
LUF7487	19.1 nM	1.5 nM	N.D.	60 nM	Antagonist	[6]
A_3						
MRS1163	145 nM (r)	272 nM (r)	N.D.	10.0 nM (r)	Agonist	[140]
SO_2F-MRS1191	41 % (100 μM) (r)	20% (100 μM) (r)	N.D.	2.42 nM	Antagonist	[141]
SO_2F-MRE-3008-F20	<5 % (100 nM)	50 nM	N.D.	79% (100 nM)	Antagonist	[142]
LUF7602	79 nM	1.3 μM	0% (10 μM)	10 nM	Antagonist	[143]

[a]The data are apparent affinities for the human adenosine receptors or % displacement at the concentration in brackets unless indicated otherwise (r = rat, b =bovine). N.D. = not determined

6. Concluding Remarks

Molecular probes, including radioligands, fluorescent and covalent ligands, are important tool compounds that facilitate the biochemical and structural investigation of GPCRs. As shown in this review, these probes provide information about the nature of adenosine receptors, next to a deeper understanding of receptor regulation and the pathological /physiological roles of this GPCR subfamily. In particular, when combined with other techniques such as receptor mutagenesis, X-ray crystallography and homology modelling, these tools provide a powerful platform for molecular receptor pharmacology.

Radioligands are the most developed tools for GPCRs. An established standard radioligand binding assay provides crucial and reliable measurements of GPCRs interacting with their synthetic ligands as well as newly developed probes. The choice of radioligands may influence the quantitative information about the measurement. Binding of an agonist radioligand may reveal different apparent affinity states depending on the receptor states (i.e. G protein-coupled and G protein-uncoupled) or cell-dependent effector coupling. Thus, antagonist radioligands are generally considered more acceptable in receptor classification than agonists. Among the adenosine receptors, there is still an urgent need for the development of better antagonist radioligands for the $A_{2B}R$ and A_3R with high affinity with K_D values of 1 nM or less, with low non-specific binding and better selectivity. For *in vivo* assays, the development of PET ligands targeting $A_{2B}R$ and A_3R has still been limited to receptor occupancy studies, biodistribution or pharmacokinetic characterization, while PET ligands for A_1R and $A_{2A}R$ have blossomed in clinical studies, particularly for neurological disorders. Studies on $A_{2B}R$ and A_3R are generally considered to be hampered by the low expression level of these receptors in endogenous tissue, insufficient affinity of the tool compound and unclear mechanisms involved in the receptor function. It is anticipated that continued efforts to develop high-affinity and selective PET tracers for adenosine receptors will further our understanding of the role these receptors have in disease conditions.

Concerns about radiation safety and shelf life have fueled the continuing interest in small-molecule fluorescent tools. Recent examples summarized in this review demonstrate that fluorescent probes represent an alternative approach to investigate AR characteristics. However, their use is still sub-optimal due to the often high level of non-specific membrane binding brought by the hydrophobic pharmacophore and fluorophore. Hence, researchers should pay more attention to designing probes with favorable physicochemical properties. Besides, the *in vivo* applications of such tools are still hampered, partly due to their short

excitation wavelengths and low tissue penetration [144]. Future development of synthetic ligands with a focus on near-infrared (NIR) fluorophores might be advantageous, especially since such wavelengths are not harmful to cells and have a relatively low absorption. Such NIR probes were already employed to study the cannabinoid CB_2 and α_1-adrenergic receptors [145, 146].

Compared to radioligand and fluorescent probes, covalent ligands do not possess any detectable functionality for direct quantification or visualization of receptors. When combined with site-direct mutagenesis, mass spectrometry and peptide sequencing, they constitute a powerful approach to study adenosine receptor subtype and structure, map ligand binding sites, investigate the physiological and pathological roles of receptors and determine the correlation between receptor occupancy and response. The emergence of the activity-based protein profiling technique inspired researchers to equip probes with click handles to yield bifunctional probes that can be used to visualize receptors for target validation. In this strategy a probe binds the receptor with less perturbation compared to relatively large tags linked to ligand scaffolds beforehand, which bridges the field of chemical biology with the field of molecular pharmacology to better investigate receptor-ligand interactions. In future research, different tags may be introduced; for instance, a biotin-tag would allow for streptavidin-mediated receptor enrichment followed by LC/MS analysis. Of note, the $A_{2B}R$ has been known as the more poorly characterized adenosine receptor subtype. This also has limited the development of molecular probes targeting $A_{2B}R$ specifically, especially for the covalently binding ligands, where no case has been reported so far. Covalent probes for $A_{2B}R$ and A_3R may also assist in the structure elucidation of these two adenosine receptor subtypes, which are currently still lacking.

For decades, scientists have been continuously developing tool compounds to study adenosine receptors. In this endeavor the use of covalent or reversible probes, whether radiolabeled or fluorescent, has been instrumental, i) to discover new chemical entities, ii) to characterize and interrogate adenosine receptor subtypes both *in vitro* and *in vivo*, and iii) to study their behavior in physiological and disease conditions. This review has summarized evidence for these applications, but, hopefully, it also serves as an invitation to walk another mile to further improve probe characteristics and develop additional tags that interrogate adenosine receptors and other GPCRs in even finer detail.

References

1. Jacobson K.A., and Gao Z.G. *Nat Rev Drug Discov.* **2006**. 5(3): 247-264.
2. Jaakola V.P., Griffith M.T., Hanson M.A., Cherezov V., Chien E.Y., Lane J.R., IJzerman A.P., and Stevens R.C. *Science.* **2008**. 322(5905): 1211-1217.
3. Glukhova A., Thal D.M., Nguyen A.T., Vecchio E.A., Jorg M., Scammells P.J., May L.T., Sexton P.M., and Christopoulos A. *Cell.* **2017**. 168(5): 867-877
4. Gregory K.J., Velagaleti R., Thal D.M., Brady R.M., Christopoulos A., Conn P.J., and Lapinsky D.J. *ACS Chem Biol.* **2016**. 11(7): 1870-1879.
5. Soethoudt M., Stolze S.C., Westphal M.V., van Stralen L., Martella A., van Rooden E.J., Guba W., Varga Z.V., Deng H., van Kasteren S.I., Grether U., IJzerman A.P., Pacher P., Carreira E.M., Overkleeft H.S., Ioan-Facsinay A., Heitman L.H., and van der Stelt M. *J Am Chem Soc.* **2018**. 140(19): 6067-6075.
6. Yang X., Michiels T.J.M., de Jong C., Soethoudt M., Dekker N., Gordon E., van der Stelt M., Heitman L.H., van der Es D., and IJzerman A.P. *J Med Chem.* **2018**. 61(17): 7892-7901.
7. Speers A.E., and Cravatt B.F. *Chem Biol.* **2004**. 11(4): 535-546.
8. Cravatt B.F., Wright A.T., and Kozarich J.W. *Annu Rev Biochem.* **2008**. 77: 383-414.
9. Flanagan C.A., *Chapter 10 - GPCR-radioligand binding assays*, in *Methods Cell Bio*, A. K. Shukla, Editor. 2016, Academic Press. p. 191-215.
10. Hulme E.C., and Trevethick M.A. *Br J Pharmacol.* **2010**. 161(6): 1219-1237.
11. Klotz K.N., Lohse M.J., Schwabe U., Cristalli G., Vittori S., and Grifantini M. *Naunyn-Schmiedebergs Archives of Pharmacology.* **1989**. 340(6): 679-683.
12. Lane J.R., Klaasse E., Lin J., van Bruchem J., Beukers M.W., and IJzerman A.P. *Biochem Pharmacol.* **2010**. 80(8): 1180-1189.
13. Klotz K.N., Hessling J., Hegler J., Owman C., Kull B., Fredholm B.B., and Lohse M.J. *Naunyn-Schmiedebergs Archives of Pharmacology.* **1998**. 357(1): 1-9.
14. Lohse M.J., Klotz K.N., Lindenbornfotinos J., Reddington M., Schwabe U., and Olsson R.A. *Naunyn-Schmiedebergs Archives of Pharmacology.* **1987**. 336(2): 204-210.
15. Xia L., de Vries H., IJzerman A.P., and Heitman L.H.H. *Purinergic Signal.* **2016**. 12(1): 115-126.
16. Jarvis M.F., Schulz R., Hutchison A.J., Do U.H., Sills M.A., and Williams M. *J Pharmacol Exp Ther.* **1989**. 251(3): 888-893.
17. Svenningsson P., Hall H., Sedvall G., and Fredholm B.B. *Synapse.* **1997**. 27(4): 322-335.
18. Kurumaji A., and Toru M. *Brain Res.* **1998**. 808(2): 320-323.
19. Wan W., Sutherland G.R., and Geiger J.D. *J Neurochem.* **1990**. 55(5): 1763-1771.
20. Lindstrom K., Ongini E., and Fredhohn B.B. *Naunyn-Schmiedeberg's Archives of Pharmacology.* **1996**. 354(4): 539-541.
21. Kim J., Wess J., van Rhee A.M., Schoneberg T., and Jacobson K.A. *J Biol Chem.* **1995**. 270(23): 13987-13997.
22. Muller C.E., Maurinsh J., and Sauer R. *Eur J Pharm Sci.* **2000**. 10(4): 259-265.
23. Sihver W., Schulze A., Wutz W., Stusgen S., Olsson R.A., Bier D., and Holschbach M.H. *Eur J Pharmacol.* **2009**. 616(1-3): 107-114.
24. Hockemeyer J., Burbiel J.C., and Muller C.E. *J Org Chem.* **2004**. 69(10): 3308-3318.
25. Alexander S.P.H., and Millns P.J. *Eur J Pharmacol.* **2001**. 411(3): 205-210.

26. Guo D., Mulder-Krieger T., IJzerman A.P., and Heitman L.H. *Br J Pharmacol.* **2012**. 166(6): 1846-1859.
27. Xiaodong J., and Jacobson K.A. *Drug Des and Discov.* **1999**. vol. 16,3 (1999): 217-226.
28. Dionisotti S., Ongini E., Zocchi C., Kull B., Arslan G., and Fredholm B.B. *Br J Pharmacol.* **1997**. 121(3): 353-360.
29. El Yacoubi M., Ledent C., Parmentier M., Ongini E., Costentin J., and Vaugeois J.M. *Eur J Neurosci.* **2001**. 14(9): 1567-1570.
30. Bryant R., McGuinness D., Turek-Etienne T., Guyer D., Yu L.M., Howells L., Caravano J., Zhai Y., and Lachowicz J. *Assay Drug Dev Technol.* **2004**. 2(3): 290-299.
31. Hinz S., Alnouri W.M., Pleiss U., and Muller C.E. *Purinergic Signal.* **2018**. 14: 223-233.
32. Casado V., Casillas T., Mallol J., Canela E.I., Lluis C., and Franco R. *J Neurochem.* **1992**. 59(2): 425-431.
33. Robeva A.S., Woodard R.L., Jin X.W., Gao Z.H., Bhattacharya S., Taylor H.E., Rosin D.L., and Linden J. *Drug Develop Res.* **1996**. 39(3-4): 243-252.
34. Bosch M.P., Campos F., Niubo I., Rosell G., Diaz J.L., Brea J., Loza M.I., and Guerrero A. *J Med Chem.* **2004**. 47(16): 4041-4053.
35. Linden J., Thai T., Figler H., Jin X., and Robeva A.S. *Mol Pharmacol.* **1999**. 56(4): 705-713.
36. Ji X.D., Kim Y.C., Ahern D.G., Linden J., and Jacobson K.A. *Biochem Pharmacol.* **2001**. 61(6): 657-663.
37. Baraldi P.G., Tabrizi M.A., Preti D., Bovero A., Fruttarolo F., Romagnoli R., Moorman A.R., Gessi S., Merighi S., Varani K., and Borea P.A. *Bioorg Med Chem Lett.* **2004**. 14(13): 3607-3610.
38. Gessi S., Varani K., Merighi S., Cattabriga E., Pancaldi C., Szabadkai Y., Rizzuto R., Klotz K.N., Leung E., Mac Lennan S., Baraldi P.G., and Borea P.A. *Mol Pharmacol.* **2005**. 67(6): 2137-2147.
39. Stewart M., Steinig A.G., Ma C.L., Song J.P., McKibben B., Castelhano A.L., and MacLennan S.J. *Biochem Pharmacol.* **2004**. 68(2): 305-312.
40. Borrmann T., Hinz S., Lertarelli D.C.G., Li W.J., Florin N.C., Scheiff A.B., and Muller C.E. *J Med Chem.* **2009**. 52(13): 3994-4006.
41. Zhou Q.Y., Li C., Olah M.E., Johnson R.A., Stiles G.L., and Civelli O. *Proc Natl Acad Sci U S A.* **1992**. 89(16): 7432-7436.
42. Olah M.E., Gallorodriguez C., Jacobson K.A., and Stiles G.L. *Mol Pharmacol.* **1994**. 45(5): 978-982.
43. Lane J.R., Beukers M.W., Mulder-Krieger T., and IJzerman A.P. *Biochem Pharmacol.* **2010**. 79(1): 48-56.
44. Klotz K.N., Falgner N., Kachler S., Lambertucci C., Vittori S., Volpini R., and Cristalli G. *Eur J Pharmacol.* **2007**. 556(1-3): 14-18.
45. Gao Z.G., Teng B., Wu H.T., Joshi B.V., Griffiths G.L., and Jacobson K.A. *Purinergic Signalling.* **2009**. 5(1): 31-37.
46. Auchampach J.A., Gizewski E.T., Wan T.C., de Castro S., Brown G.G., and Jacobson K.A. *Biochem Pharmacol.* **2010**. 79(7): 967-973.
47. Varani K., Merighi S., Gessi S., Klotz K.N., Leung E., Baraldi P.G., Cacciari B., Romagnoli R., Spalluto G., and Borea P.A. *Mol Pharmacol.* **2000**. 57(5): 968-975.
48. Baraldi P.G., Cacciari B., Romagnoli R., Varani K., Merighi S., Gessi S., Borea P.A., Leung E., Hickey S.L., and Spalluto G. *Bioorg Med Chem Lett.* **2000**. 10(3): 209-211.

49. Muller C.E., Diekmann M., Thorand M., and Ozola V. *Bioorg Med Chem Lett.* **2002**. 12(3): 501-503.
50. Beukers M.W., Chang L.C., von Frijtag Drabbe Kunzel J.K., Mulder-Krieger T., Spanjersberg R.F., Brussee J., and IJzerman A.P. *J Med Chem.* **2004**. 47(15): 3707-3709.
51. Mishina M., and Ishiwata K. *Int Rev Neurobiol.* **2014**. 119: 51-69.
52. Khanapur S., Waarde A., Ishiwata K., Leenders K.L., Dierckx R.A., and Elsinga P.H. *Curr Med Chem.* **2014**. 21(3): 312-328.
53. van Waarde A., Dierckx R., Zhou X., Khanapur S., Tsukada H., Ishiwata K., Luurtsema G., de Vries E.F.J., and Elsinga P.H. *Med Res Rev.* **2018**. 38(1): 5-56.
54. Paul S., Elsinga P.H., Ishiwata K., Dierckx R.A.J.O., and van Waarde A. *Curr Med Chem.* **2011**. 18(31): 4820-4835.
55. Fukumitsu N., Ishii K., Kimura Y., Oda K., Sasaki T., Mori Y., and Ishiwata K. *J Nucl Med.* **2005**. 46(1): 32-37.
56. Bauer A., Holschbach M.H., Meyer P.T., Boy C., Herzog H., Olsson R.A., Coenen H.H., and Zilles K. *Neuroimage.* **2003**. 19(4): 1760-1769.
57. Meyer P.T., Elmenhorst D., Boy C., Winz O., Matusch A., Zilles K., and Bauer A. *Neurobiol Aging.* **2007**. 28(12): 1914-1924.
58. Elmenhorst D., Elmenhorst E.M., Hennecke E., Kroll T., Matusch A., Aeschbach D., and Bauer A. *P Natl Acad Sci USA.* **2017**. 114(16): 4243-4248.
59. Elmenhorst D., Meyer P.T., Matusch A., Winz O.H., and Bauer A. *J Nucl Med.* **2012**. 53(11): 1723-1729.
60. Mishina M., Ishii K., Kimura Y., Suzuki M., Kitamura S., Ishibashi K., Sakata M., Oda K., Kobayashi S., Kimura K., and Ishiwata K. *Synapse.* **2017**. 71(8).
61. Matusch A., Saft C., Elmenhorst D., Kraus P.H., Gold R., Hartung H.P., and Bauer A. *Eur J Nucl Med Mol Imaging.* **2014**. 41(6): 1210-1220.
62. Guo M., Gao Z.-G., Tyler R., Stodden T., Li Y., Ramsey J., Zhao W.-J., Wang G.-J., Wiers C.E., Fowler J.S., Rice K.C., Jacobson K.A., Kim S.W., and Volkow N.D. *J Med Chem.* **2018**. 61(22): 9966-9975.
63. Mishina M., Ishiwata K., Naganawa M., Kimura Y., Kitamura S., Suzuki M., Hashimoto M., Ishibashi K., Oda K., Sakata M., Hamamoto M., Kobayashi S., Katayama Y., and Ishii K. *PLoS One.* **2011**. 6(2): 17338.
64. Mishina M., Ishiwata K., Kimura Y., Naganawa M., Oda K., Kobayashi S., Katayama Y., and Ishii K. *Synapse.* **2007**. 61(9): 778-784.
65. Ramlackhansingh A.F., Bose S.K., Ahmed I., Turkheimer F.E., Pavese N., and Brooks D.J. *Neurology.* **2011**. 76(21): 1811-1816.
66. Moresco R.M., Todde S., Belloli S., Simonelli P., Panzacchi A., Rigamonti M., Galli-Kienle M., and Fazio F. *Eur J Nucl Med Mol Imaging.* **2005**. 32(4): 405-413.
67. Zhou X., Khanapur S., Huizing A.P., Zijlma R., Schepers M., Dierckx R.A., van Waarde A., de Vries E.F., and Elsinga P.H. *J Med Chem.* **2014**. 57(21): 9204-9210.
68. Ishibashi K., Miura Y., Wagatsuma K., Toyohara J., Ishiwata K., and Ishii K. *Neuropharmacology.* **2018**. 143: 106-112.
69. Khanapur S., Paul S., Shah A., Vatakuti S., Koole M.J.B., Zijlma R., Dierckx R.A.J.O., Luurtsema G., Garg P., van Waarde A., and Elsinga P.H. *J Med Chem.* **2014**. 57(15): 6765-6780.
70. Tavares A.A., Batis J.C., Papin C., Jennings D., Alagille D., Russell D.S., Vala C., Lee H., Baldwin R.M., Zubal I.G., Marek K.L., Seibyl J.P., Barret O., and Tamagnan G.D. *J Nucl Med.* **2013**. 54(10): 1760-1767.

71. Barret O., Hannestad J., Vala C., Alagille D., Tavares A., Laruelle M., Jennings D., Marek K., Russell D., Seibyl J., and Tamagnan G. *J Nucl Med.* **2015**. 56(4): 586-591.

72. Petroni D., Giacomelli C., Taliani S., Barresi E., Robello M., Daniele S., Bartoli A., Burchielli S., Pardini S., Salvadori P.A., Da Settimo F., Martini C., Trincavelli M.L., and Menichetti L. *Nucl Med Biol.* **2016**. 43(5): 309-317.

73. Lindemann M., Hinz S., Deuther-Conrad W., Namasivayam V., Dukic-Stefanovic S., Teodoro R., Toussaint M., Kranz M., Juhl C., Steinbach J., Brust P., Muller C.E., and Wenzel B. *Bioorg Med Chem.* **2018**. 26(16): 4650-4663.

74. Li A.-H., Moro S., Forsyth N., Melman N., Ji X.-d., and Jacobson K.A. *J Med Chem.* **1999**. 42(4): 706-721.

75. Wadsak W., Mien L.-K., Shanab K., Ettlinger D.E., Haeusler D., Sindelar K., Lanzenberger R.R., Spreitzer H., Viernstein H., Keppler B.K., Dudczak R., Kletter K., and Mitterhauser M. *Nuclear Medicine and Biology.* **2008**. 35(1): 61-66.

76. Wadsak W., Mien L.K., Shanab K., Ettlinger D.E., Haeusler D., Sindelar K., Lanzenberger R.R., Spreitzer H., Viernstein H., Keppler B.K., Dudczak R., Kletter K., and Mitterhauser M. *Nucl Med Biol.* **2008**. 35(1): 61-66.

77. Balber T., Singer J., Berroteran-Infante N., Dumanic M., Fetty L., Fazekas-Singer J., Vraka C., Nics L., Bergmann M., Pallitsch K., Spreitzer H., Wadsak W., Hacker M., Jensen-Jarolim E., Viernstein H., and Mitterhauser M. *Contrast Media Mol Imaging.* **2018**.

78. Mitterhauser M., Haeusler D., Mien L.-K., Ungersboeck J., Nics L., Lanzenberger R.R., Sindelar K., Viernstein H., Dudczak R., and Kletter K. *Open Nucl Med J.* **2009**. 1: 15-23.

79. Kiesewetter D.O., Lang L., Ma Y., Bhattacharjee A.K., Gao Z.-G., Joshi B.V., Melman A., de Castro S., and Jacobson K.A. *Nuclear Medicine and Biology.* **2009**. 36(1): 3-10.

80. Ishiwata K., Ogi N., Shimada J., Nonaka H., Tanaka A., Suzuki F., and Senda M. *Ann Nucl Med.* **2000**. 14(2): 81-89.

81. Todde S., Moresco R.M., Simonelli F., Baraldi P.G., Cacciari B., Spalluto G., Varani K., Monopoli A., Matarrese M., Carpinelli A., Magni F., Kienle M.G., and Fazio F. *J Med Chem.* **2000**. 43(23): 4359-4362.

82. Neustadt B.R., Hao J., Lindo N., Greenlee W.J., Stamford A.W., Tulshian D., Ongini E., Hunter J., Monopoli A., Bertorelli R., Foster C., Arik L., Lachowicz J., Ng K., and Feng K.-I. *Bioorg Med Chem Lett.* **2007**. 17(5): 1376-1380.

83. Shinkre B.A., Kumar T.S., Gao Z.G., Deflorian F., Jacobson K.A., and Trenkle W.C. *Bioorg Med Chem Lett.* **2010**. 20(19): 5690-5694.

84. Kumar T.S., Mishra S., Deflorian F., Yoo L.S., Phan K., Kecskes M., Szabo A., Shinkre B., Gao Z.G., Trenkle W., and Jacobson K.A. *Bioorg Med Chem Lett.* **2011**. 21(9): 2740-2745.

85. Vala C., Morley T.J., Zhang X., Papin C., Tavares A.A., Lee H.S., Constantinescu C., Barret O., Carroll V.M., Baldwin R.M., Tamagnan G.D., and Alagille D. *ChemMedChem.* **2016**. 11(17): 1936-1943.

86. Kozma E., Jayasekara P.S., Squarcialupi L., Paoletta S., Moro S., Federico S., Spalluto G., and Jacobson K.A. *Bioorg Med Chem.* **2013**. 23(1): 26-36.

87. Stoddart L.A., Vernall A.J., Denman J.L., Briddon S.J., Kellam B., and Hill S.J. *Chem Biol.* **2012**. 19(9): 1105-1115.

88. Arruda M.A., Stoddart L.A., Gherbi K., Briddon S.J., Kellam B., and Hill S.J. *Front Pharmacol.* **2017**. 8: 908.

89. Briddon S.J., Middleton R.J., Cordeaux Y., Flavin F.M., Weinstein J.A., George M.W., Kellam B., and Hill S.J. *Proc Natl Acad Sci U S A.* **2004**. 101(13): 4673-4678.

90. Cooper S.L., Soave M., Jorg M., Scammells P.J., Woolard J., and Hill S.J. *Br J Pharmacol.* **2019**. 176(7): 864-878.

91. Fernandez-Duenas V., Gomez-Soler M., Jacobson K.A., Kumar S.T., Fuxe K., Borroto-Escuela D.O., and Ciruela F. *J Neurochem.* **2012**. 123(3): 373-384.

92. Fernandez-Duenas V., Gomez-Soler M., Morato X., Nunez F., Das A., Kumar T.S., Jauma S., Jacobson K.A., and Ciruela F. *Neurochemistry International.* **2013**. 63(1): 42-46.

93. McCabe R.T., Skolnick P., and Jacobson K.A. *J Fluoresc.* **1992**. 2(4): 217-223.

94. McNeely P.M., Naranjo A.N., Forsten-Williams K., and Robinson A.S. *Slas Discovery.* **2017**. 22(2): 166-175.

95. Duroux R., Ciancetta A., Mannes P., Yu J.H., Boyapati S., Gizewski E., Yous S., Ciruela F., Auchampach J.A., Gao Z.G., and Jacobson K.A. *Medchemcomm.* **2017**. 8(8): 1659-1667.

96. Kose M., Gollos S., Karcz T., Fiene A., Heisig F., Behrenswerth A., Kiec-Kononowicz K., Namasivayam V., and Muller C.E. *J Med Chem.* **2018**. 61(10): 4301-4316.

97. Barresi E., Giacomelli C., Daniele S., Tonazzini I., Robello M., Salerno S., Piano I., Cosimelli B., Greco G., Da Settimo F., Martini C., Trincavelli M.L., and Taliani S. *Bba-Biomembranes.* **2018**. 26(22): 5885-5895.

98. Corriden R., Self T., Akong-Moore K., Nizet V., Kellam B., Briddon S.J., and Hill S.J. *Embo Reports.* **2013**. 14(8): 726-732.

99. Vernall A.J., Stoddart L.A., Briddon S.J., Ng H.W., Laughton C.A., Doughty S.W., Hill S.J., and Kellam B. *Org Biomol Chem.* **2013**. 11(34): 5673-5682.

100. Stoddart L.A., Vernall A.J., Briddon S.J., Kellam B., and Hill S.J. *Neuropharmacology.* **2015**. 98: 68-77.

101. Kozma E., Kumar T.S., Federico S., Phan K., Balasubramanian R., Gao Z.G., Paoletta S., Moro S., Spalluto G., and Jacobson K.A. *Biochem Pharmacol.* **2012**. 83(11): 1552-1561.

102. Jorg M., and Scammells P.J. *ChemMedChem.* **2016**. 11(14): 1488-1498.

103. Adeniyi A.A., Muthusamy R., and Soliman M.E. *Expert Opin Drug Discov.* **2016**. 11(1): 79-90.

104. Robinette D., Neamati N., Tomer K.B., and Borchers C.H. *Expert Rev. Proteomics.* **2006**. 3(4): 399-408.

105. Grunbeck A., and Sakmar T.P. *Biochem.* **2013**. 52(48): 8625-8632.

106. Dorman G., and Prestwich G.D. *Trends Biotechnol.* **2000**. 18(2): 64-77.

107. Morey T.E., Belardinelli L., and Dennis D.M. *Br J Pharmacol.* **1998**. 123(7): 1425-1433.

108. Yasunaga T., Motoyama S., Nose T., Kodama H., Kondo M., and Shimohigashi Y. *J Biol Chem.* **1996**. 120(2): 459-465.

109. Weichert D., and Gmeiner P. *Acs Chem Biol.* **2015**. 10(6): 1376-1386.

110. Stiles G.L., Daly D.T., and Olsson R.A. *J Biol Chem.* **1985**. 33(2): A231-A231.

111. Klotz K.N., Cristalli G., Grifantini M., Vittori S., and Lohse M.J. *J Biol Chem.* **1985**. 260(27): 4659-4664.

112. Lohse M.J., Klotz K.N., and Schwabe U. *Mol Pharmacol.* **1986**. 30(4): 403-409.

113. Lohse M.J., Klotz K.N., and Schwabe U. *Mol Pharmacol.* **1991**. 39(4): 517-523.

114. Earl C.Q., Patel A., Craig R.H., Daluge S.M., and Linden J. *J Med Chem.* **1988**. 31(4): 752-756.

115. Kennedy A.P., Mangum K.C., Linden J., and Wells J.N. *Mol Pharmacol.* **1996**. 50(4): 789-798.

116. Patel A., Craig R.H., Daluge S.M., and Linden J. *Mol Pharmacol.* **1988**. 33: 585-591.

117. Jacobson K.A., Barone S., Kammula U., and Stiles G.L. *J Med Chem.* **1989**. 32(5): 1043-1051.

118. Jorg M., Glukhova A., Abdul-Ridha A., Vecchio E.A., Nguyen A.T.N., Sexton P.M., White P.J., May L.T., Christopoulos A., and Scammells P.J. *J Med Chem.* **2016**. 59(24): 11182-11194.
119. Zhang J., Belardinelli L., Jacobson K.A., Otero D.H., and Baker S.P. *Mol Pharmacol.* **1997**. 52(3): 491-498.
120. Dennis D., Jacobson K., and Belardinelli L. *Am J Physiol.* **1992**. 262(3 Pt 2): 661-671.
121. Scammells P.J., Baker S.P., Belardinelli L., and Olsson R.A. *J Med Chem.* **1994**. 37(17): 2704-2712.
122. Gesztelyi R., Kiss Z., Wachal Z., Juhasz B., Bombicz M., Csepanyi E., Pak K., Zsuga J., Papp C., Galajda Z., Branzaniuc K., Porszasz R., Szentmiklosi A.J., and Tosaki A. *Arch Pharm Res.* **2013**. 36(3): 293-305.
123. van Muijlwijk-Koezen J.E., Timmerman H., van der Sluis R.P., van de Stolpe A.C., Menge W.M., Beukers M.W., van der Graaf P.H., de Groote M., and IJzerman A.P. *Bioorg Med Chem Lett.* **2001**. 11(6): 815-818.
124. Beauglehole A.R., Baker S.P., and Scammells P.J. *J Med Chem.* **2000**. 43(26): 4973-4980.
125. Beauglehole A.R., Baker S.P., and Scammells P.J. *Bioorg Med Chem Lett.* **2002**. 12(21): 3179-3182.
126. Barrington W.W., Jacobson K.A., Hutchison A.J., Williams M., and Stiles G.L. *Proc Natl Acad Sci U S A.* **1989**. 86(17): 6572-6576.
127. Jacobson K.A., Pannell L.K., Ji X.D., Jarvis M.F., Williams M., Hutchison A.J., Barrington W.W., and Stiles G.L. *J Mol Recognit.* **1989**. 2(4): 170-178.
128. Barrington W.W., Jacobson K.A., and Stiles G.L. *Mol Pharmacol.* **1990**. 38(2): 177-183.
129. Piersen C.E., True C.D., and Wells J.N. *Mol Pharmacol.* **1994**. 45(5): 871-877.
130. Luthin D.R., Lee K.S., Okonkwo D., Zhang P.J., and Linden J. *J Neurochem.* **1995**. 65(5): 2072-2079.
131. Baraldi P.G., Cacciari B., Spalluto G., Pineda de las Infantas y Villatoro M.J., Zocchi C., Dionisotti S., and Ongini E. *J Med Chem.* **1996**. 39(5): 1164-1171.
132. Silverman L.S., Caldwell J.P., Greenlee W.J., Kiselgof E., Matasi J.J., Tulshian D.B., Arik L., Foster C., Bertorelli R., Monopoli A., and Ongini E. *Bioorg Med Chem Lett.* **2007**. 17(6): 1659-1662.
133. Muranaka H., Momose T., Handa C., and Ozawa T. *ACS Med Chem Lett.* **2017**. 8(6): 660-665.
134. Jacobson K.A., Stiles G.L., and Ji X.D. *Mol Pharmacol.* **1992**. 42(1): 123-133.
135. Niiya K., Jacobson K.A., Silvia S.K., and Olsson R.A. *N-S Arch Pharmacol.* **1993**. 347(5): 521-526.
136. Moss S.M., Jayasekara P.S., Paoletta S., Gao Z.G., and Jacobson K.A. *ACS Med Chem Lett.* **2014**. 5(9): 1043-1048.
137. Ji X.D., Gallo-Rodriguez C., and Jacobson K.A. *Drug Develop Res.* **1993**. 29(4): 292-298.
138. Shryock J.C., Snowdy S., Baraldi P.G., Cacciari B., Spalluto G., Monopoli A., Ongini E., Baker S.P., and Belardinelli L. *Circulation.* **1998**. 98(7): 711-718.
139. Yang X., Dong G., Michiels T.J.M., Lenselink E.B., Heitman L., Louvel J., and IJzerman A.P. *Purinergic Signal.* **2017**. 13(2): 191-201.
140. Ji X.D., Gallo-Rodriguez C., and Jacobson K.A. *Biochem Biophys Res Commun.* **1994**. 203(1): 570-576.
141. Li A.H., Chang L., Ji X., Melman N., and Jacobson K.A. *Bioconjug Chem.* **1999**. 10(4): 667-677.

142. Baraldi P.G., Cacciari B., Moro S., Romagnoli R., Ji X., Jacobson K.A., Gessi S., Borea P.A., and Spalluto G. *J Med Chem.* **2001**. 44(17): 2735-2742.

143. Yang X., van Veldhoven J.P.D., Offringa J., Kuiper B.J., Lenselink E.B., Heitman L.H., van der Es D., and IJzerman A.P. *J Med Chem.* **2019**. 62(7): 3539-3552.

144. Iliopoulos-Tsoutsouvas C., Kulkarni R.N., Makriyannis A., and Nikas S.P. *Expert Opin Drug Discov.* **2018**. 13(10): 933-947.

145. Ma Z., Lin Y., Cheng Y., Wu W., Cai R., Chen S., Shi B., Han B., Shi X., Zhou Y., Du L., and Li M. *J Med Chem.* **2016**. 59(5): 2151-2162.

146. Zhang S.J., Shao P., and Bai M.F. *Bioconjug Chem.* **2013**. 24(11): 1907-191